

BACHELOR THESIS

Development and first test of a novel three-dimensional beam monitor

Author

Andreas Gsponer

Supervisor

Prof. Dr. Saverio Braccini

September 2019

UNIVERSITY OF BERN

ALBERT EINSTEIN CENTER FOR FUNDAMENTAL PHYSICS
LABORATORY FOR HIGH ENERGY PHYSICS

Contents

1. Cyclotrons and beam monitoring	2
1.1. Introduction to cyclotrons	2
1.2. Cyclotron physics	3
1.3. The PET-cyclotron at the University Hospital in Bern	3
1.4. Mini-PET beamline	4
1.5. Beam monitoring devices	5
2. The π^3 detector prototype	8
2.1. Hardware	8
2.2. Software	13
3. Laboratory tests	18
3.1. Experimental setup	18
3.2. Experimental results with a laser beam	19
3.3. Vacuum testing	22
4. First beam tests	23
4.1. Experimental Setup	23
4.2. Preliminary cyclotron testing	24
4.3. Results of the first measurement campaign	26
4.4. Results of the second measurement campaign	32
4.5. Possible improvements to the π^3 detector	42
5. Conclusions and outlook	44
Appendices	47
A. Source code	47
B. Manual of the π^3 detector	47
B.1. Setup	47
B.2. Performing a measurement	47
B.3. Preparing the analysis	48
B.4. Analyzing measurements	49

Introduction

Cyclotrons are widely used in research and medicine, mostly for the production of radioisotopes for medical imaging or for hadrontherapy, where cancer is treated by irradiation with proton beams. The medical cyclotron located at the SWAN house of the Insel hospital in Bern is used for multidisciplinary research and for radioisotope production (¹⁸fluoro-deoxy-glucose, FDG) used in Positron Emission Tomography (PET). As the demands for more precise beams have been steadily increasing, better cyclotrons and beam monitoring devices have to be developed. In hadrontherapy, it is very important to know the beam position and energy to ensure a safe and effective irradiation of the cancer being treated. In the production of radioisotopes, the target samples can be very small given their large price, so very precise and focused beams are required for an effective irradiation. Knowledge of the beam current is also important to control the amount of radioisotope produced.

The Laboratory for High Energy Physics (LHEP) at the Albert Einstein Center for Fundamental Physics (AEC) in Bern is developing a new three-dimensional beam monitor called π^3 . It is based on a scintillating screen and a camera mounted on a moving support and is able to reconstruct the beam distribution and envelope in three dimensions. The π^3 project is the next evolution of the π^2 monitor, which laid the foundation for some of technology used in this project.

In this thesis, the development of the π^3 detector as well as the laboratory tests at LHEP and the first beam tests at the Bern medical cyclotron are presented. In the first chapter, a short overview of the working principle of a cyclotron and of various beam monitoring devices used at the Bern medical cyclotron is given. The second chapter introduces the π^3 and its hardware components. The conception and realization of the software controlling the π^3 detector and analyzing the measurements is also reported. Chapter 3 presents the laboratory tests at LHEP performed in order to assess the detectors accuracy. In chapter 4, the tests and results of the measurements performed with the proton beam of the Bern medical cyclotron are presented and discussed. Finally, possible further improvements to the detector hardware and software are reported and an outlook for the possible next applications of the π^3 monitor is given.

1. Cyclotrons and beam monitoring

1.1. Introduction to cyclotrons

The first cyclotron particle accelerator was built by Ernest Lawrence together with Stanley Livingston in 1932. With this first small scale prototype, they were able to accelerate protons to 13 keV[1]. Using more powerful magnets, the acceleration energy was improved very quickly, reaching a beam energy of 8.55 MeV with a current of 100 μ A in 1938 [1]. This energy range enabled a wide palette of new science, for example by providing radioisotope tracers for medicine and biology, creating the first transuranic elements in nuclear physics and by being used in the first neutron therapy program. In the following years, the widespread usage of cyclotrons and the better theoretical understanding thereof lead to more advanced types of accelerators, including synchrotrons and isosynchronous cyclotrons, which provided even higher energy beams with numerous new applications.

In its simplest realization, a cyclotron consists of a pair of charged plates, similar to a capacitor. In the gap between the plates, the electric field accelerates the particle. This setup is limited by the maximum electric field which can be obtained and the only way to reach higher energies is to pass many times through the same gap by keeping the particles on a circular orbit. This is accomplished by the use of a dipole magnet, which bends the particles onto a spiral path. The two D-shaped electrodes, called *dees*, are driven by an alternating electric voltage and create the acceleration gap inside the cyclotron. They can be seen in Fig. 1. Every time the charged particle goes through the acceleration gap, it gets a "kick" and its energy increases. This reuse of the acceleration gap can significantly reduce the space requirements and allow cyclotrons to be installed in hospitals. Nowadays, cyclotrons are viewed as reliable and easy to use particle accelerators with many different applications.

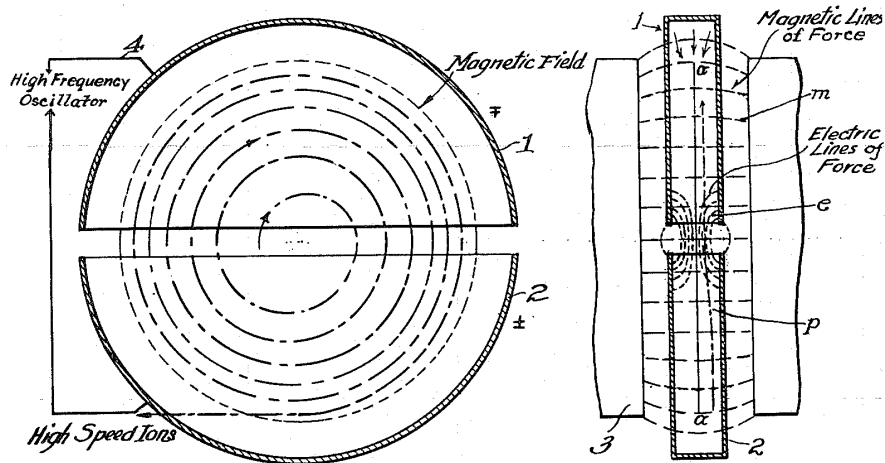


Figure 1: Original sketch of a cyclotron from Ernest Lawrence's patent [2]

1.2. Cyclotron physics

A particle in a cyclotron experiences the magnetic component of the Lorentz force and the centripetal force, which have to be equal for the particle to be in a stable orbit:

$$qvB = \frac{mv^2}{r}, \quad (1.2.1)$$

where q is the charge of the particle, v is the velocity of the particle, B the applied magnetic field, m the mass of the particle and r the radius of the cyclotron. In order for the particle to travel one revolution around the cyclotron, it needs to travel a distance of $2\pi r$. The time T needed to travel this distance can be calculated by using the velocity calculated in equation (1.2.1):

$$T = \frac{2\pi r}{v} = \frac{2\pi r}{\frac{qBr}{m}} = \frac{2\pi m}{qB}. \quad (1.2.2)$$

From this rotation period, the so called cyclotron frequency f is given by

$$f = \frac{1}{T} = \frac{qB}{2\pi m}. \quad (1.2.3)$$

It is important to note here that the cyclotron frequency does not depend on the speed of the particle or the radius of the cyclotron. This means that with the same cyclotron frequency, the particle will be in a stable orbit in all stages of the acceleration.

An effect which has to be considered for high energies is that the mass of the particle increases relativistically with its velocity. The equation (1.2.3) then needs to be modified to take this effect into account:

$$f = \frac{1}{T} = \frac{qB}{2\pi m\gamma(v)}, \quad (1.2.4)$$

with $\gamma(v)$ being the Lorentz factor given by $1/\sqrt{1-v^2/c^2}$. If this correction is neglected, the cyclotron frequency will not match the particles with higher energies, meaning that the acceleration will get out of tune and stop working or even decelerate particles. One way to avoid this problem is to vary the magnetic field radially to compensate the gamma factor, keeping the cyclotron frequency constant.

1.3. The PET-cyclotron at the University Hospital in Bern

The cyclotron in the SWAN facility at the University Hospital in Bern is used for PET isotope production and multidisciplinary research. Thanks to a beam transfer line (BTL) placed in a second bunker separated from the cyclotron one, research and production can be performed in parallel, even if there is still radiation left in the cyclotron bunker after radioisotope production. This is a rare feature uncommon to cyclotrons in hospitals.

The cyclotron itself can accelerate H^- ions to 18 MeV and was built by Ion Beam Applications (IBA) in Belgium. With a carbon stripping foil, the electrons of the H^- ions are stripped away, leaving a proton which is guided by the magnetic field

out of the cyclotron. The average magnetic field is 1.4 T [3] which gives a cyclotron frequency of 21 MHz. After extraction out of the cyclotron, the proton beam either heads towards a production target inside the cyclotron bunker or goes on in the BTL to the research bunker. The BTL, depicted in Fig. 2, features two horizontal-vertical quadrupole doublets and an XY-steering magnet, which can control the beam size and position allowing for varying beam sizes from centimeters to a few millimeters. It is important that the beam is well focused and aligned to the axis of the BTL, in order to reduce beam losses and to limit unwanted activation.

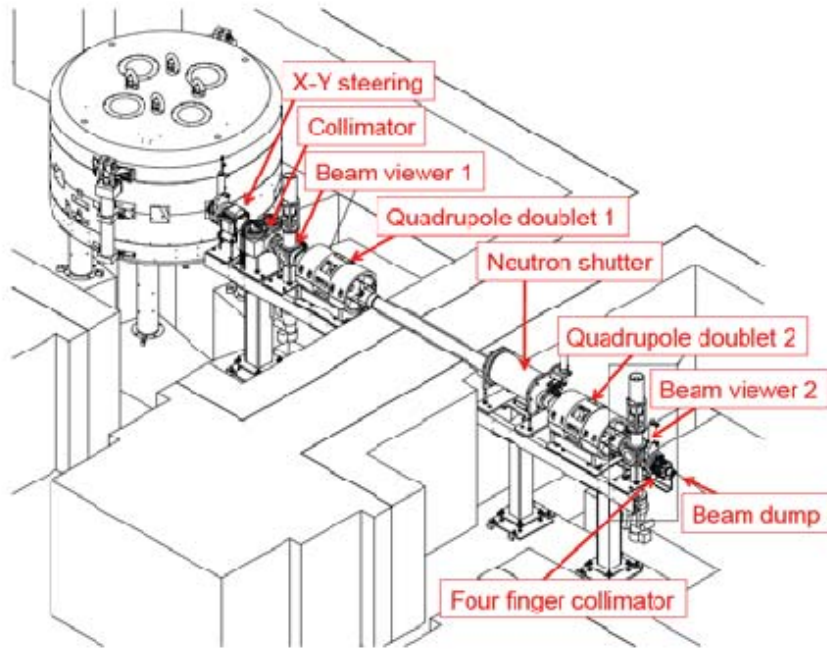


Figure 2: Schematic of the beam transfer line in the Bern medical cyclotron [3]

1.4. Mini-PET beamline

The Mini-Pet Beamline (MBL), shown in Fig. 3, is a compact beamline of 1.6 m length. It features a quadropole doublet and two steering magnets, which focus and displace the beam in the horizontal and vertical plane. The position of the magnets is adjustable which increases the amount of possible configurations of the beamline. Together with the beam control of the BTL, this allows for very precise control over the proton beam and can be used to improve the beam quality and to produce a wide diversity of beams. The ability to manipulate the beam further is very useful when testing or calibrating new beam monitors, as the effect of beam focusing or steering can be controlled and compared to the monitor readout. The MBL provides the structural support to the π^3 detector, which is mounted on it and can be moved throughout the MBL. As the MBL features an uncommon non-circular beam pipe, additional challenges were present in designing a mechanical system able to move the π^3 detector throughout the MBL.



Figure 3: Rendering of the Mini-PET beamline [4].

1.5. Beam monitoring devices

Beam monitors are very important in particle accelerators, as they are used in tuning and controlling beam parameters such as beam position, size or current. For example in hadrontherapy, the localization of the beam is very important in order to only irradiate part of the tissue where cancer is present while avoiding excess irradiation of healthy tissue. In order to calculate the necessary irradiation time of a patient, the beam current also must be precisely known and is not permitted to fluctuate.

Beam monitors can be divided into two main groups, destructive and non-destructive monitors, each with their own advantages and disadvantages. Destructive monitors such as Faraday cups have a significant influence on the beam, which prevents the usage of the monitor at the same time an irradiation is conducted. Destructive beam monitors are mainly used to measure or tune beam parameters which will stay the same in different runs and do not depend on the type of target chosen.

Non-(or nearly non-)destructive beam monitors allow the beam to be conserved and can provide information about the beam while an irradiation is ongoing, which is essential for safety monitoring. Depending on how non-destructive the monitor is, a number of them can be used at the same time in order to provide even more information of the beam. Both types of monitors, destructive and non-destructive, used at the Bern medical cyclotron will be briefly introduced in the following.

1.5.1. Faraday cup

A Faraday cup is one of the simplest types of beam monitors and was already used in the first operating cyclotron built by Lawrence and Livingston [5]. A Faraday cup can catch charged particles, and measure the beam current on the detector. Faraday cups are destructive monitors so they are mounted at the end of the beam

line. Since the beam can have a high power, a Faraday cup needs to be constantly cooled down. One challenge for Faraday cups is to make sure that no electrons produced by secondary emission can escape the cup, which would lead to a reduced beam current being measured. In order to avoid this issue, an electric field can be used to push the particles back into the cup, which captures the secondary electrons. With Faraday cups, very accurate measurements can be made, with a sensitivity of down to a few pA. They are very widely used given their high accuracy and the beam current being one of the most important parameters of the beam.

1.5.2. UniBEaM

The UniBEaM (Universal Beam Monitor) detector, developed by LHEP at the University of Bern, is a special type of wire scanner. It is based on two scintillating fibers introduced into the beam path, which can be moved in the X and Y plane by stepper motors. When the beam hits the scintillating fibers, photons are produced which are guided to a photo multiplier providing a digital readout and the amount of photons measured directly correlates with the beam intensity integrated along the fiber. By performing horizontal and vertical sweeps with the fibers, X and Y profiles of the beam can be obtained with the stepper motors enabling a spatial resolution of about 0.1 mm.

One of the main advantages of using a scintillating fiber over traditional wire scanners, which work by measuring the charge deposited by the beam or produced by secondary emission, is that the scintillating fiber used by the UniBEaM can measure beams with currents as low as 1 pA, opposed to 1 μ A for traditional wire scanners.

Also, the electronics of the UniBEaM can be placed far away of the detector, which eliminates any radiation hardness problems and increases the lifetime of the detector. Furthermore, the scintillating fibers are nearly non-destructive and allow measurements during irradiation with negligible interference. The commercial version of the UniBEaM produced under license by the Canadian manufacturer D-PACE¹, features two fibers mounted perpendicularly, has a spatial resolution of up to 25 μ m and has a linear fiber response in respect to beam current in the range of 1 pA to 3 μ A[6]. The integrated area of the measured 2D beam profiles is directly proportional to the beam current.

1.5.3. π^2 monitor

The π^2 detector is a type of scintillating screen monitor and was also developed by LHEP at the University of Bern [7, 8]. Here, an aluminum foil is coated with a scintillating material converting a part of the energy deposited by the beam into visible light, which can then be viewed by a camera. In the π^2 monitor, an aluminum screen coated with the scintillating compound P47 was used and mounted with an angle of 45° from the beam path and viewed by a camera installed on a

¹<https://www.d-pace.com/>

view port. The π^2 monitor and its main components can be seen in Fig. 4. Depending on the thickness of the screen and the materials used, scintillating screens can have different degrees of beam destructiveness. This monitor is able to instantaneously measure the two dimensional profile of the beam, and reconstruct the beam current in a similar way as the UniBEaM does. As shown in [8], the scintillating screen used in the π^2 monitor is practically non-destructive but can scatter protons non-negligibly for broad beam profiles. The response of the scintillating screen is linear for currents below 300 pA. The π^3 monitor is based on this detector and will be presented in the next chapter.

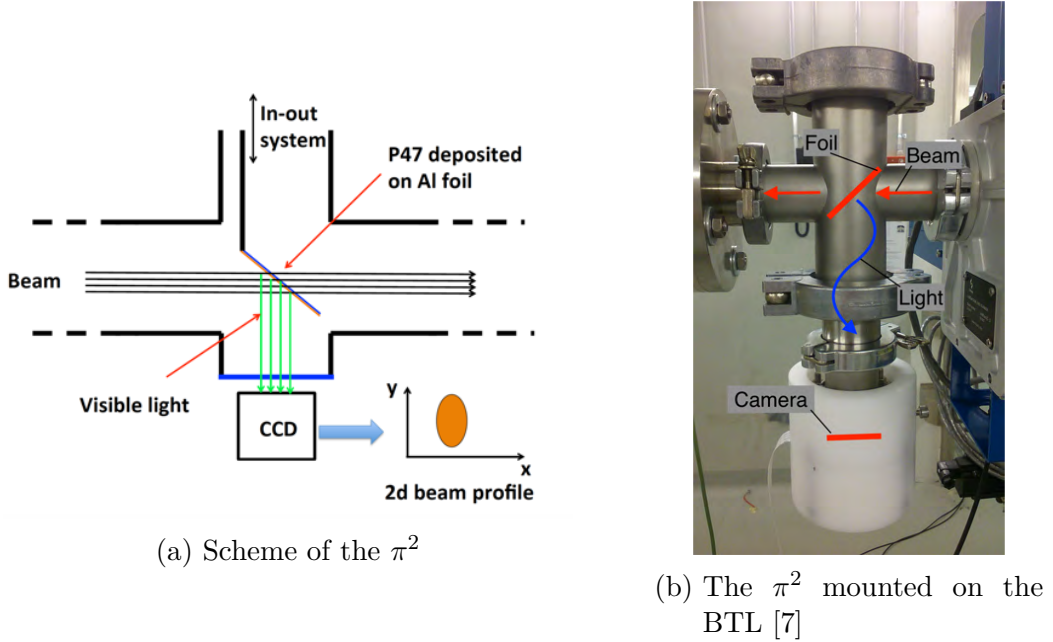


Figure 4: Scheme (a) and photograph (b) of the π^2 monitor.

2. The π^3 detector prototype

The π^3 detector is integrated into the Mini-PET beamline (MBL) and was designed and constructed by the LHEP workshop. The monitor has been designed to measure beam cross sections with a scintillating foil similarly as the π^2 monitor does, with the difference being that the scintillating foil and camera are mounted on a movable support. By moving this support throughout the MBL, the beam shape and position can be measured along the length of the MBL, as well as a 3D representation of the beam envelope can be obtained. The scintillating foil used for measuring the beam is nearly non-destructive, but the current mechanical construction of the π^3 uses an aluminum flange to mount the motor moving the foil and camera support, stopping the beam at the end of the MBL. In this chapter, both the hardware and software components of the π^3 monitor are introduced.

2.1. Hardware

The main components of the π^3 monitor are the scintillating screen, the camera and the moving support with its motor. All of these components are mounted inside the MBL, as shown in Fig. 5. The moving support (1) carries the scintillating screen and the camera. It can be moved by a stepper motor (2) which is connected to the support via a vacuum feedtrough and a 66 cm long screw (3). The inserts drawn

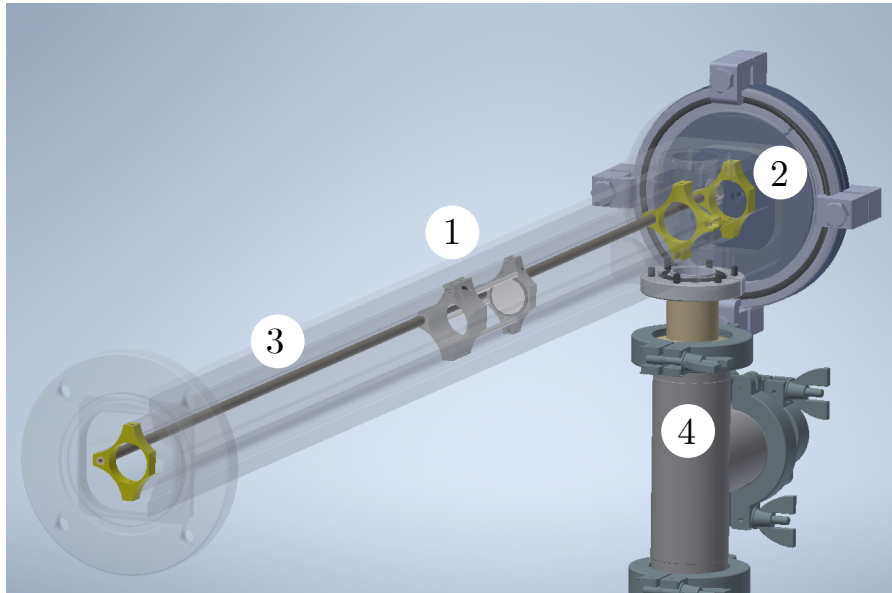


Figure 5: Overview of the π^3 mounted inside of the MBL.

in yellow at the beginning and end of the MBL are used to keep the assembly in place. At the end of the beam pipe, a vacuum tube is mounted perpendicularly (4) which is used for the cable puller system described later on. Not visible in this drawing are the integrated magnets of the MBL. The length that the support can move and perform measurements is 660 mm. In the following, the individual parts of the π^3 are explained in detail.

2.1.1. Scintillating screen

The moving support features a screen holder (visible in Fig. 6), which allows circular targets consisting of different materials to be mounted. For the preliminary tests, a simple paper screen was used to view a laser beam. In order to view the proton beam produced by a cyclotron, an aluminum foil coated with the scintillating compound P47 is used. This foil converts part of the energy of the protons into light, which can be recorded by a camera operating in the visual range. The

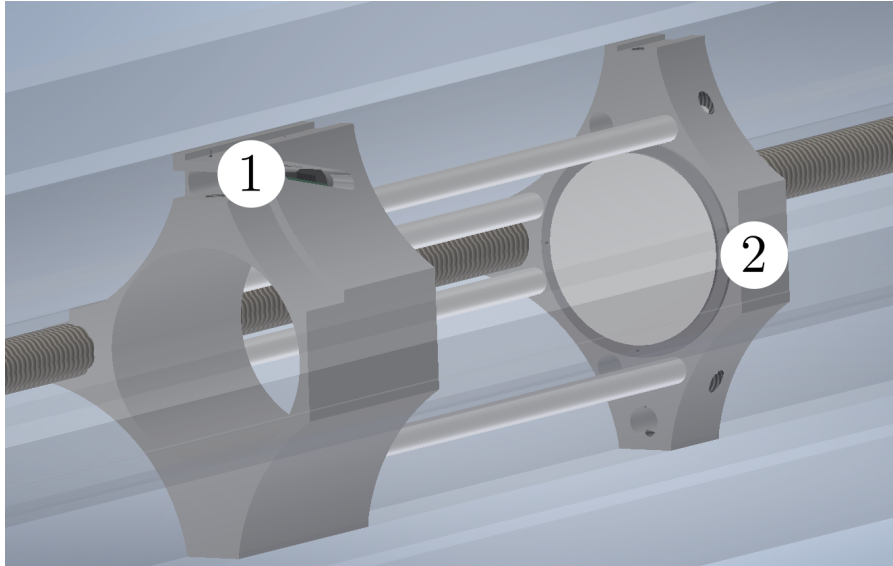


Figure 6: Drawing of the moving support, complete with the camera (1) and the target screen (2).

P47 compound and foil used are similar as those used in the π^2 monitor, but with a smaller diameter foil and thicker coating. The energy conversion spectrum is given in Fig. 7, which shows that the expected light of P47 is blue in color. The decay time of P47 (from 90 % to 10 % Luminescence) is 100 ns [9]. Compared to the frame rate of the camera, which is the amount of pictures the camera can record in a second, this decay time is negligible and therefore has no influence in the measurements.

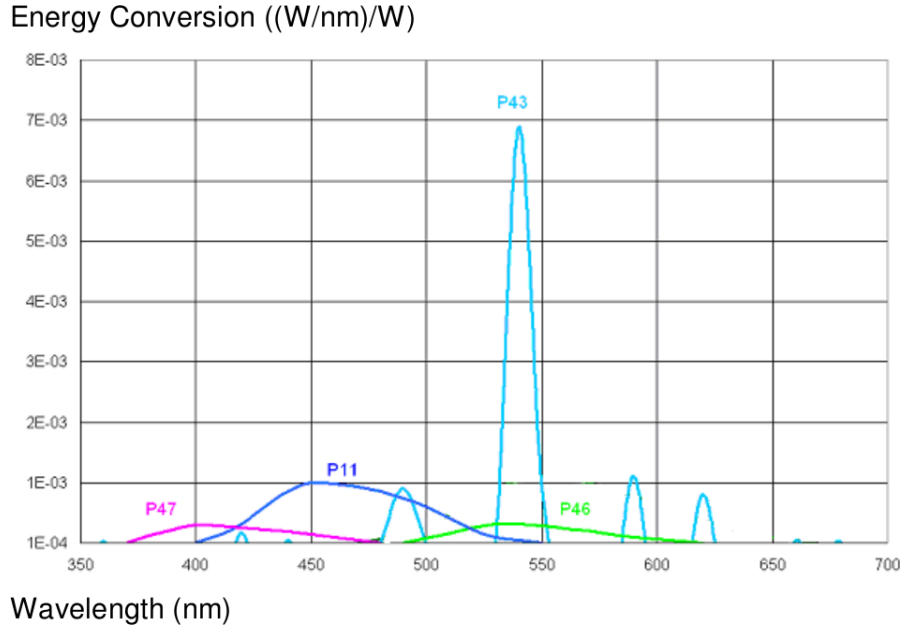


Figure 7: Energy conversion for P47 and related phosphor compounds [9].

2.1.2. Camera

The camera used was extracted from an inexpensive USB endoscope camera system². It has a diameter of 5 mm. The resolution of this camera is 640×480 px and it can record video at 8 frames per second. The camera ISO³ and exposure time cannot be adjusted manually. The low cost of this camera is crucial, as it is exposed to vacuum and can be damaged by radiation and scattered particles, with neutrons being the most destructive. A ring of LED lights is present on the camera, which can be controlled by software and used for a visual inspection of the foil or other components without the need for disassembly. Both the USB connection of the camera and the LED power cable are connected via a vacuum feedtrough to a Raspberry Pi computer, which can record videos and control the LED ring.

One of the issues encountered with the camera is its heat production. When in usage, the camera draws about 0.5 W of power, which heats up the small body of the camera considerably after less than 5 min. The thermal issues are intensified in vacuum, where heat transfer is impaired. The contact area between the camera and its support mount is very small and insufficient for adequate heat conduction. It was found that the thermal issues can lead to image degradation, manifesting in the image turning red and the thermal noise being increased.

In order to fix these thermal issues, the heat conduction between the camera and its support had to be enhanced. Multiple thermally conducting compounds were evaluated, but were rejected because of their insufficient vacuum properties (excessive degassing) when heated or complicated application. Because of the low durability of the cameras used, an easy to apply and remove solution was

²"KKmoon 5mm 2m Mini Digital USB Endoscope Inspection Camera"

³A measure related to the sensitivity of the camera



Figure 8: The view of the camera onto the scintillating foil, illuminated by the LED ring. On the foil, the four corner points used in image preprocessing are visible.

preferred. Thermal gap filler pads, commonly used in electronics for connecting heat sinks to uneven surfaces, fulfilled these criteria and is very easy to apply and remove. By cutting up the pads and filling the space between the camera and its support, sufficient thermal conduction was achieved. The vacuum tests conducted (see chapter 3.3), showed sufficient vacuum properties of the thermal pads. With this setup, the camera can be used continuously for at least 10 min without image degradation.

Because the camera is mounted at a slight angle with respect to the scintillating foil, the image perspective needs to be corrected by software (see chapter 2.2.4). This can be done by marking points on the screen defining four corners of a square, visible as circles of missing coating in Fig. 8. These points allow the software to correct the camera angle, by mapping the corner points onto a perfect square. With the setup used in the cyclotron tests, the rectangle defined by the four corner points is of size $340 \pm 5 \text{ px} \times 245 \pm 5 \text{ px}$. The diameter of the scintillating foil is $23.6 \pm 0.1 \text{ mm}$, and the biggest square fitting in this circle therefore has edges of length $16.7 \pm 0.1 \text{ mm}$. This means that the π^3 monitor has a maximal horizontal resolution of $0.05 \pm 0.01 \text{ mm px}^{-1}$ and a maximal vertical resolution of $0.07 \pm 0.01 \text{ mm px}^{-1}$.

The distance between the camera support and the screen support can be adjusted, which can change the spatial resolution of the monitor. In the tests, the camera was moved as close as possible to the screen in order to achieve a maximal resolution. Using a camera featuring a higher resolution, this spatial resolution could easily be increased.

2.1.3. Computer

The computer powering the π^3 monitor is a Raspberry Pi 3 Model B+ ⁴, a low cost, credit card sized computer featuring general purpose input/output (GPIO) pins. The GPIO pins can be connected to different types of HAT (Hardware Attached on Top), which in this case features a PWM controller able to move the motor and control the position of the scintillating foil inside the MBL. Also, by using the integrated, low power PWM controller of the Raspberry Pi, the LED lighting of the camera can be controlled and dimmed by software. The Raspberry Pi used features a Broadcom BCM2837B0, Cortex-A53 64-bit SoC @ 1.4GHz with 1GB of LPDDR2 SDRAM.

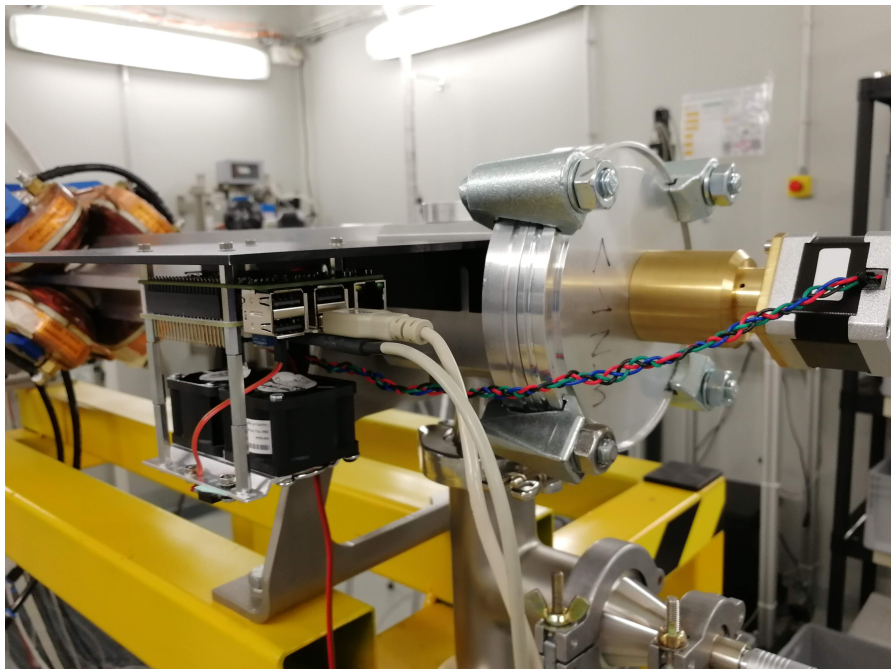


Figure 9: The Raspberry Pi mounted onto the MBL with the HAT and cooling attached. At the right side, the stepper motor moving the scintillating screen is visible.

2.1.4. Movable support

The movable support featuring the scintillating screen and camera is connected to a long screw located all along the MBL. This screw is connected to a stepper motor, which moves the support 1 mm per revolution and can perform very small steps of up to a 1/100th rotation. Very small steps of the motor were not used because at full speed, moving the monitor through the 660 mm already requires up to 3 min and longer measurement times would be unpractical. The screw has manufacturing imperfections and is not entirely straight, which can be noticed by a rattling sound when the screw hits the MBL wall during rotations.

⁴<https://www.raspberrypi.org/products/raspberry-pi-3-model-b-plus/>

One of the main issues of the moving support is that there is a space ($< 1 \text{ mm}$) between it and the MBL wall, leading to the support having play and the position of the support not being exactly known anymore. Investigation and characterization of this was one of the primary goals in the preliminary tests (see chapter 3.1).

The stepper motor is connected to a PWM controller which interfaces with the Raspberry Pi and needs to provide a considerable amount of power (25 W) during movement. When performing multiple passes throughout the MBL, the PWM controller can overheat and shutdown to protect itself. In order to avoid this issue, heat sinks were added and additional fans were put in place allowing the motor to be used indefinitely without overheating.

In order to transmit data and power to the moving support, a cable connects the USB camera and LED lights to the Raspberry Pi via a vacuum feedtrough. This cable needs to move with the support and is not allowed tangle up or interfere with the beam. To control the cable in a fixed position, two different systems were evaluated. The first system consisted of two carbon rails confining the camera cable in one of the MBL grooves. This system was unsuccessful, because the carbon rails used were not stiff enough, which resulted in them flexing and not properly constraining the cable.

The system used successfully is a gravity based system, where a weight inside a second vacuum tube is attached to the cable via a puller, providing tension and pulling the cable down when the support is moved backwards. In order to avoid collision with the end of the MBL and to allow for a homing of the support, a switch was installed which is depressed when the weight in the puller system is low enough.

2.2. Software

The programming language chosen for this project is Python, which provides useful libraries for image processing and hardware interfacing. The source code for the software used in performing measurements and analysis can be found in appendix A and was developed in the framework of this Bachelor thesis.

To conduct a measurement, the support is moved a specific distance and the camera view is recorded at the same time, which can be analyzed after preprocessing is applied. The goal of the analysis is to fit a Gaussian distribution to all of the individual cross sections to define the beam shape at any position inside the MBL. This Gaussian distribution describes the beam by the mean defining the beam center and the covariance matrix defining the shape of the beam. From the diagonal of the covariance matrix the standard deviation σ in both x and y axis can be calculated, which is directly connected to the β -function commonly used in beam dynamics⁵. The individual parts of the analysis and measurement software are detailed in the next subsections.

⁵Assuming a constant beam emittance ϵ , the β -function is given by $\beta = \sigma^2/\epsilon$.

2.2.1. Generating sample images

In order to test the accuracy of the analysis software, images of beam cross sections with controlled parameters had to be generated. This allowed the analysis software to be tested before the π^3 hardware was available. To generate these beam cross sections, it is assumed that the beam is Gaussian in nature, which means that an image can be generated by plotting a multivariate Gaussian distribution. Using the `scipy.stats`⁶ and `Pillow`⁷ python packages, images looking very similar to real images taken by the π^2 monitor can be created, visible in Fig. 10. Since the

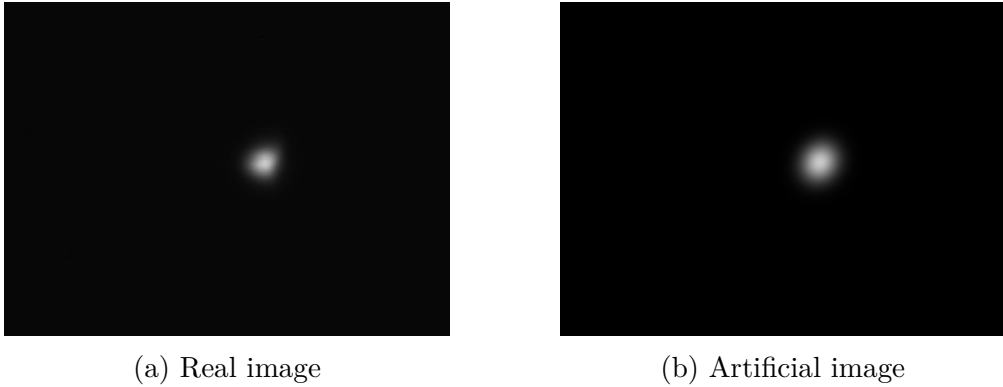


Figure 10: Real image taken by the π^2 monitor and artificial image used in testing.

parameters of the Gaussian distribution are known when creating the image, the accuracy of the analysis software can be measured by comparing the original with the reconstructed Gaussian parameters.

2.2.2. Fitting a Gaussian distribution to an image

In order to fit a Gaussian distribution to the measurement data, the image is first converted into a matrix of pixel intensities, either by extracting a single color or by averaging the three colors. The center of the Gaussian distribution μ (corresponding to the beam center) can be estimated as

$$\vec{\mu} = \frac{1}{N} \sum_{i,j} (\hat{x}i + \hat{y}j) \cdot I_{ij}, \quad (2.2.1)$$

where \hat{x} and \hat{y} are the unit vectors in the x and y directions, I_{ij} is the intensity of the pixel at (i, j) and N is the total amount of pixels. The elements of the covariance matrix can be calculated as

$$\Sigma_{jk} = \frac{1}{N} \sum_{i=1}^N (\mathbf{X}_{ij} - \vec{\mu}_j)(\mathbf{X}_{ik} - \vec{\mu}_k), \quad (2.2.2)$$

with \mathbf{X} being the matrix of pixel intensities. The covariance matrix provides information about the shape of the Gaussian distribution, with the diagonal elements being the standard deviation squared. Fig. 11 shows a cross section from

⁶<https://scipy.org/>

⁷<https://python-pillow.org/>

the cyclotron tests, fitted with a Gaussian distribution and the two principal components of its covariance matrix. The python library `numpy`⁸ provides an efficient implementation for calculating the weighted mean and covariance of arbitrary dimensional matrices.

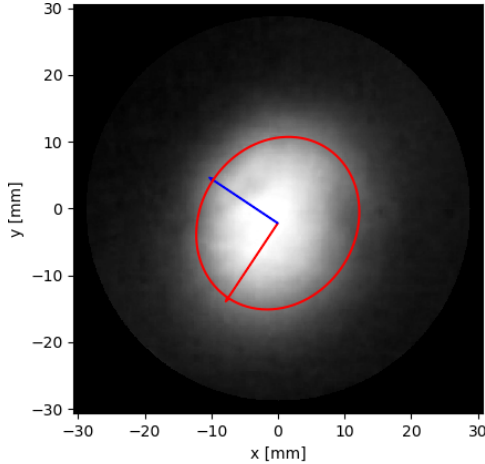


Figure 11: Fitted Gaussian on a cross section from a cyclotron measurement. The $1-\sigma$ contour of the Gaussian and the two principal components (eigen-vectors of the covariance matrix) are visible in the image.

2.2.3. Reconstructing the 3D beam envelope

Because the isocontours of a Gaussian are ellipses, the 3D beam envelope can be specified by a parameterized ellipse in direction of the beam axis. The major and minor axis are then given by the standard deviation in x and y, and the ellipse is centered in the mean of the cross section. This only works for diagonal covariance matrixes, so in order to consider a possible 2D rotation of the ellipses and account for non diagonal covariance matrices, a rotation angle can be introduced to the the ellipse parameterization. This rotation angle can be calculated from the eigenvectors of the covariance matrix and with this, the beam envelope can be accurately reconstructed in 3D from individual cross sections. In order to achieve a continuous beam envelope from the measurements, parameters of the ellipses at the measured points are interpolated with smooth cubic splines. Fig. 12 shows a smooth 3D reconstruction from only four fitted cross sections. Because of the noise which can be present in the cross section parameters, a moving average is applied first to the data before fitting the ellipse parameters.

2.2.4. Image preprocessing

In order to analyze the measurements, the data first needs to be converted in a format suitable for the analysis software and different error corrections need to be applied. The most important of these corrections is to rectify the image distortion generated by the angle of the camera respective to the screen. For this purpose, 4

⁸<https://numpy.org/>

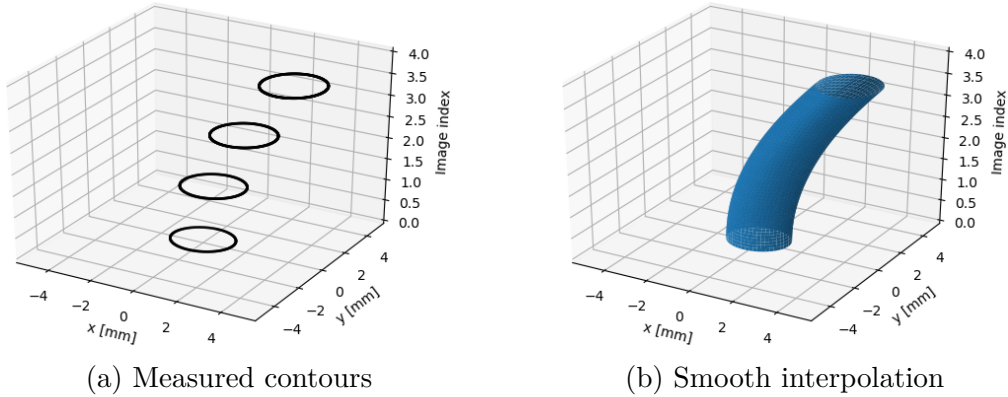


Figure 12: Example of the interpolation used to obtain a smooth beam envelope

corner points are drawn onto or etched in the target screen. These 4 points form a square and the target screen is inserted in a way that the edges of this square are aligned to the x and y axis of the beamline. By using OpenCV⁹, a transformation matrix can be found which maps these 4 corner points to a non distorted square. Applying this transformation matrix to the entire image, the perspective can be corrected and a top-down view of the target screen can be obtained.

One thing to consider is that the parts of the screen which are further away from the camera than others (as a result of the screen not being parallel relative to the camera) take up less pixels than parts of the screen which are closer to the camera. This means that in the image preprocessing, when the perspective is corrected, not all parts of the screen have the same spatial resolution. Pixels of parts of the screen which are further away from the camera get stretched more than pixels of parts close to the screen and therefore the spatial resolution is not identical for all parts of the image. Because of the small viewing angle of the camera ($< 10^\circ$) this effect was neglected. Fig. 13 shows the individual steps of the preprocessing for an image taken in a cyclotron measurement. Another correction applied is to use a threshold to cut off very high and low intensity parts of the image. The low intensity cutoff was used to remove reflections from the MBL walls and to remove the laser infrared halo present in the preliminary tests. The high intensity cutoff was used in the cyclotron measurements to remove white streaks of stray neutrons and protons, which saturate the pixels they hit. Finally, a circular mask is applied to the image using OpenCV, which removes every part of the image not on the screen. A manual detailing the usage of the control and analysis software can be found in appendix B. The software of the π^3 monitor allows for the measured beam center positions and covariance matrices to be exported in CSV format for further analysis.

⁹<https://opencv.org/>

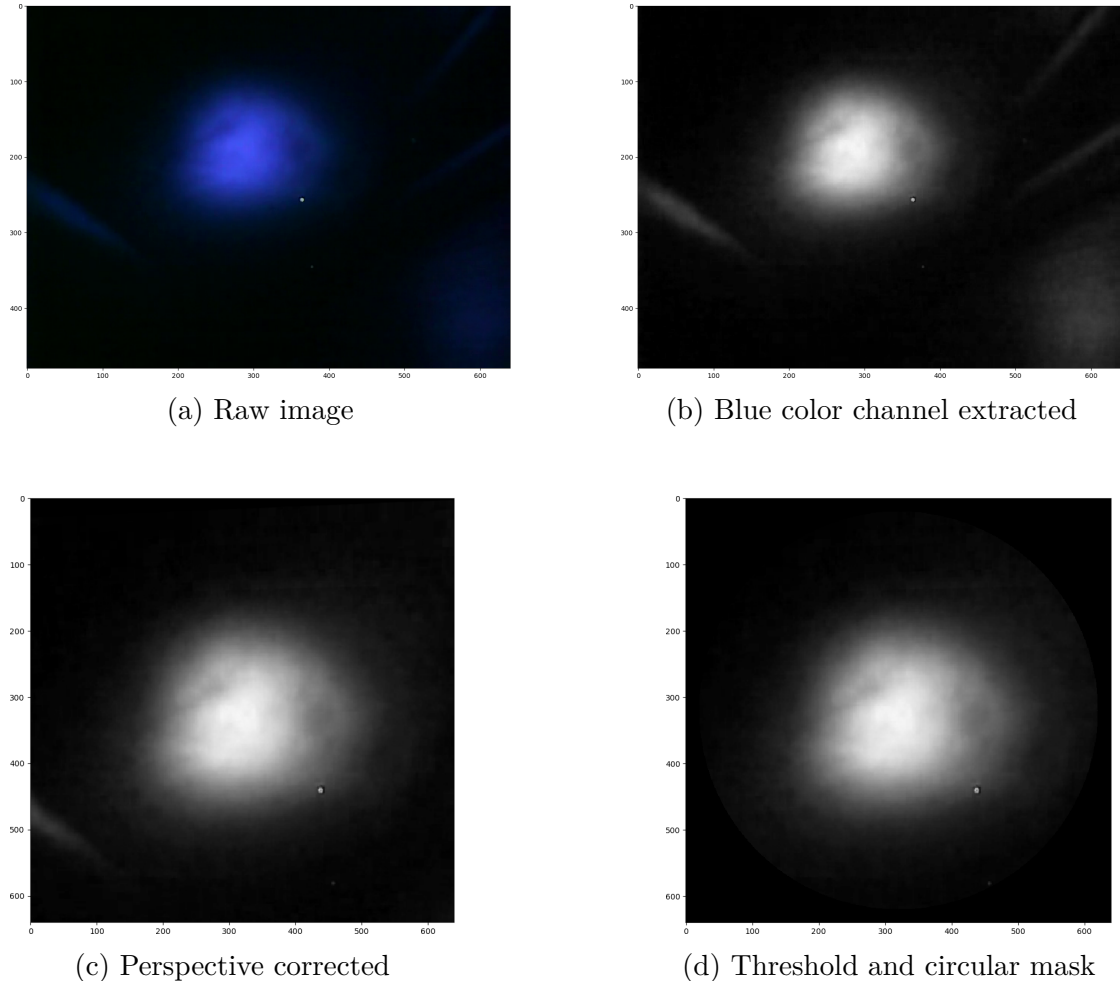


Figure 13: The different stages of preprocessing used to prepare the images for analysis.

3. Laboratory tests

3.1. Experimental setup

Before the π^3 monitor was tested with a proton beam at the cyclotron, it was evaluated in a simplified and controlled environment in the laboratory at LHEP. By fitting the target screen with a piece of paper and using a simple handheld laser mounted on a vice a proton beam could be simulated. Because this requires the beam pipe to be opened for the laser beam, no vacuum was present in the preliminary tests.

The main goal of this test was to determine if the position of the moving support (and its target screen) is accurate and not affected by the mechanical play. Also, the measurement and analysis software was able to be tested in similar conditions as in the measurements with the cyclotron. The first idea for checking the position of the moving support was to align the laser in the center of the MBL and to measure the center position of the beam as seen by the detector. Any error in the position of the moving support from the MBL axis would be visible as a deviation of the beam center position from zero. In practice, the laser was not able to be mounted with the desired accuracy without a specially machined mount. Instead it was decided to purposely misalign the laser (as seen in Fig. 14), which meant that the beam center moved in x and y by the distance inside the MBL. By calculating the deviation of the beam center position by distance from a straight line, the error of the support position could be measured. The laser was misaligned in a way that the beam spot moved diagonally from one corner of the screen to the other when moved throughout the MBL. This way, the movement of the beam center position is maximal and any deviations from a linear movement are magnified.

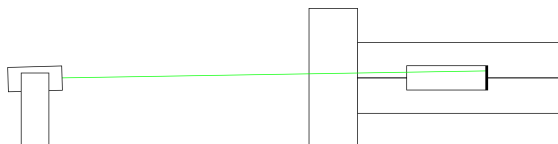


Figure 14: Experimental setup for the preliminary tests. The green laser at the left side produces a misaligned beam of light, which hits the screen of the π^3 .

In Fig. 15a one of the first images taken in the preliminary tests is shown. A red halo can be seen around the laser dot, which is unexpected for a green laser. This red halo is infrared light and originates in the way the green light is produced in the laser. First, infrared light is generated with a wavelength of 1064 nm, which is then sent to a frequency doubling crystal converting the light to 532 nm (green light). Because the conversion efficiency of this frequency doubling crystal is not perfect (and can be rather low in practice), some light will stay at an infrared wavelength. Normally, this remaining infrared light is absorbed by an infrared filter, but this filter is often missing in inexpensive lasers [10]. This infrared halo also interfered with the analysis of the images taken by the π^3 monitor. In order to avoid this halo, a point-like aperture was added to the laser and image preprocessing was

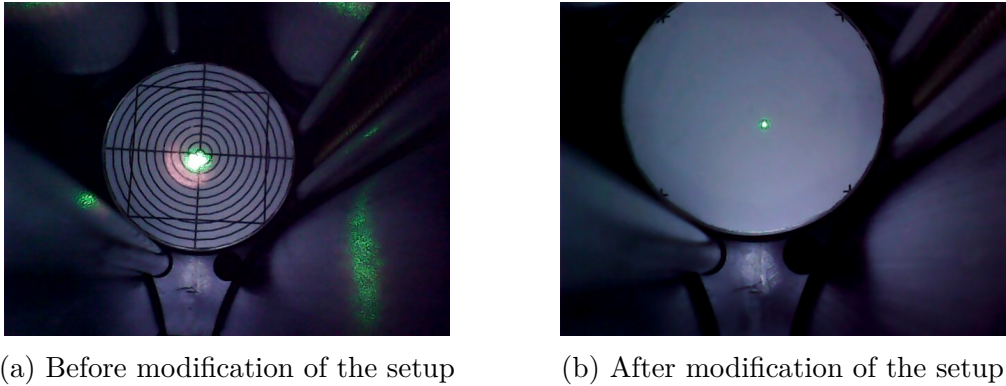


Figure 15: Camera view of the target screen with the initial and improved experimental setup.

applied, which reduced the infrared halo significantly. Also, the aperture reduced the laser beam intensity on the screen, which helped to reduce overexposure of the camera. In addition to this, the target screen was modified to only include the four corner points necessary for perspective correction, visible in the modified experimental setup in Fig. 15b. For the preliminary measurements, the laser was aligned as detailed before and the screen π^3 was moved multiple times throughout the length of the MBL, while video of the target screen was recorded for every pass.

3.2. Experimental results with a laser beam

With the modified setup, the preliminary measurements could be successfully conducted. Fig. 16 shows the movement of the beam center in both the horizontal and vertical axis by the distance inside the MBL, which is clearly linear. The position does not change by the same distance in both axis, because the laser was not perfectly aligned to both axis. By using a linear fit and determining the distance of the measurement data to this fit, the error of the beam position can be evaluated. Fig. 17 shows the deviation of the beam center from a linear movement.

This deviation is randomly distributed and very small ($< 1 \text{ mm}$). Multiple measurements produce different results, but are all randomly distributed with a maximal deviation lower than 0.3 mm . Therefore, the accuracy of the detector in the horizontal and vertical plane (on the scintillating screen) is evaluated to be 0.3 mm , which corresponds to around 5 px on the captured image. The accuracy of the detector in the axis along the beamline (z) is assumed to be 1 mm , which corresponds to one rotation of the screw. The stepper motor is capable of even smaller movements ($1/100$ rotations), but the accuracy of the screw construction is a limiting factor. An possible error in the z position of the screen during the previous assessment of the x/y accuracy does not impact the measurement. With the beam spot moving a total distance of $50.5 \pm 0.3 \text{ mm}$, the beam spot moves about 0.07 mm per mm moved in the z axis along the MBL. This possible error is therefore smaller than the error measured in the x/y plane.

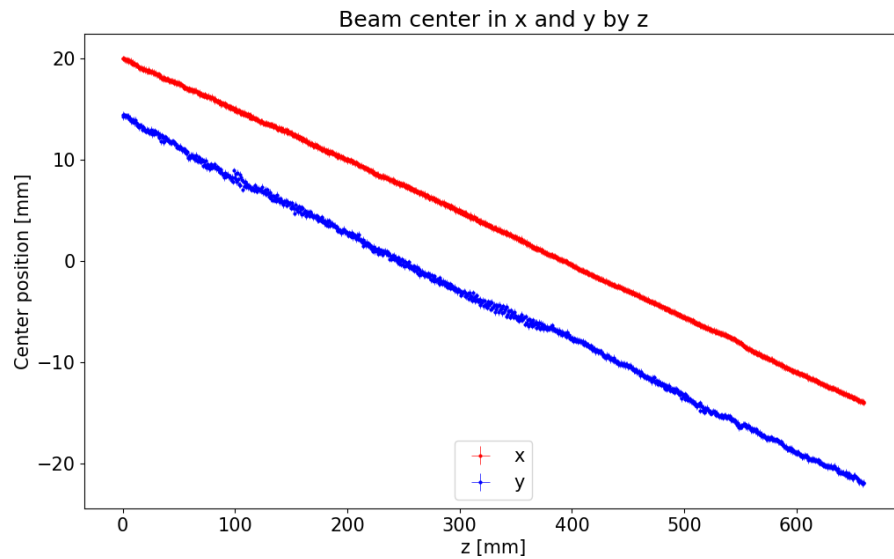


Figure 16: Position of the beam center in the horizontal (x) and vertical (y) axis by the distance along the MBL (z). Because of the density of the data points, the individual error bars are not clearly visible.

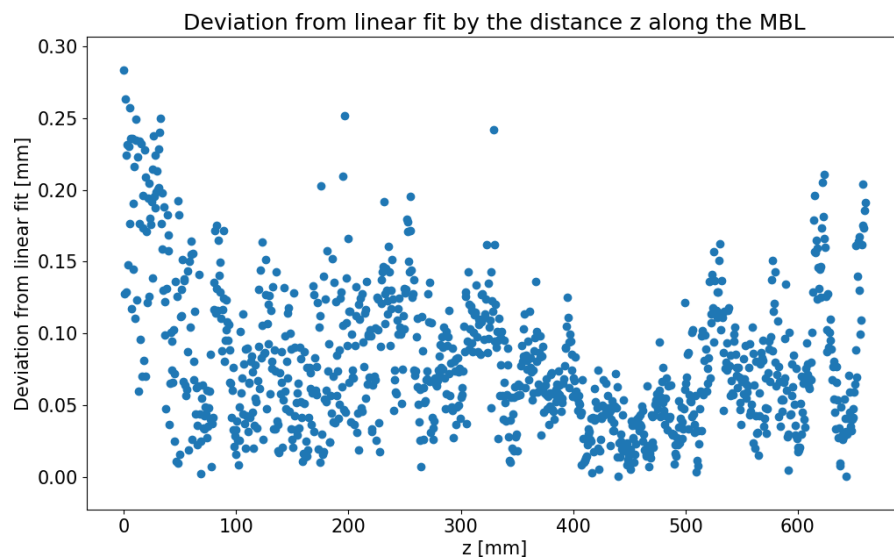


Figure 17: Measured deviation of the beam center movement from a linear fit.

In Fig. 18, the standard deviation in both axis is shown which increases with distance as the laser beam expands. The standard deviation is not the same for both axis, because the beam spot is not entirely circular as the aperture used was created by poking a hole in black tape and therefore is not perfect. Also, the width of the beam is very small (less than 20 px), which is why there is a considerable amount of noise present in the data. This noise can be clearly seen in the standard deviation for the first 200 mm of the movement. This is a feature of the laser and the effect is not present in the measurements with the proton beam.

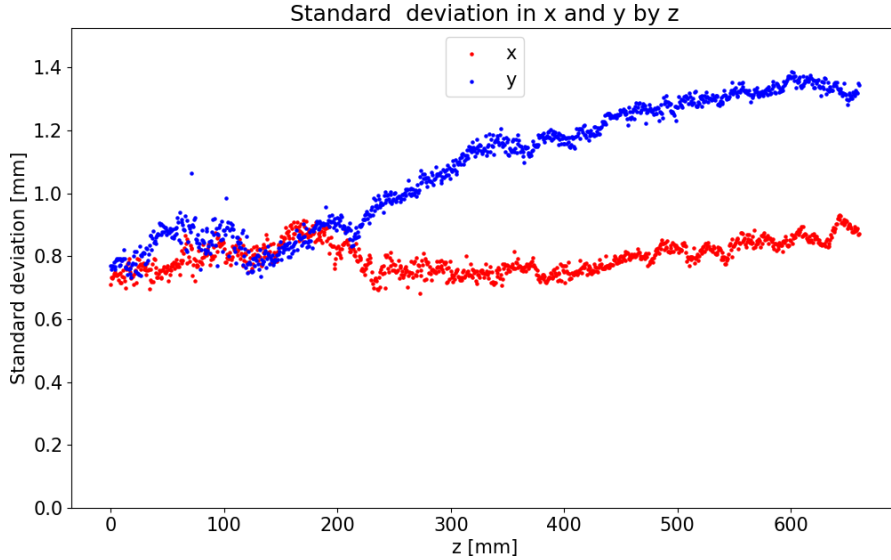


Figure 18: Standard deviation in both axis by the distance along the MBL.

One thing to note is that this experiment only checks for random errors in the positional accuracy of the detector. Systematic errors in the detector may still be present, for example if the MBL is mounted inaccurately in relation to the beamline axis or if the corner points on the target screen used in image preprocessing are inaccurate. For the mounting process of the MBL to the beamline, alignment lasers are used to try and minimize this error. With an positional error of only 0.3 mm, the π^3 system proved to be very accurate spatially.

3.3. Vacuum testing

Because the beamline in the cyclotron features high vacuum (on the order of 10^{-6} mbar), vacuum tightness and low outgassing of the π^3 monitor and its components had to be carefully tested. To conduct vacuum tests inside of the LHEP workshop, a Pfeiffer HiCube vacuum pump was used. For the experiments, the π^3 assembly was pumped for at least an hour until the vacuum pressure reached an equilibrium. For the experiment, the LED light of the camera was enabled and multiple videos of 5 min duration were recorded. While the recording was ongoing, the vacuum pressure was measured regularly to watch for outgassing problems. The first vacuum test conducted revealed that the camera suffered from thermal issues after 2 min of operating, as shown in Fig. 19. Because the camera can't dissipate heat as it does in air, the camera overheats and the camera image degrades to an unusable state. Also, some of the cameras used in the experiments showed a permanently blurred image after being exposed to vacuum, which is caused by the vacuum disarranging the camera lens. As the motor requires up to 3 min to move

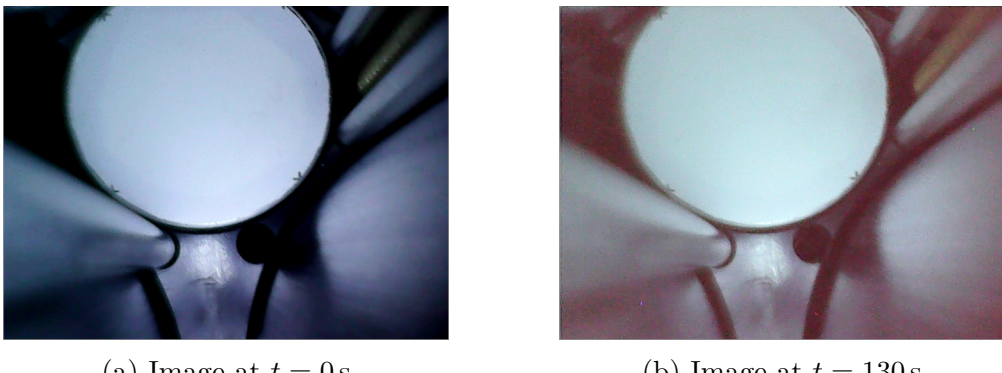


Figure 19: View of a paper target screen in vacuum at different stages of pumping, highlighting the thermal degradation of the image quality. A blur of the image can be noticed caused by the vacuum disarranging the camera lens.

through the length of the MBL the camera image would degrade to an unusable state before one measurement is completed. Therefore, a thermal solution allowing heat conduction between the camera and its support was needed. Multiple thermal solutions were evaluated but found inadequate concerning their thermal and vacuum properties or their ease of application. The successful thermal gap filler pads, described in chapter 2.1.2, were installed and the same vacuum tests were repeated. This experiment showed that, starting with a pressure of 1.9×10^{-4} mbar, the pressure increased only slightly to 2.2×10^{-4} mbar after 30 s of camera usage, but did not increase any further. The camera image showed no signs of thermal degradation for at least 10 min, which allows for multiple measurements to be performed before a cooling break is necessary. The vacuum achieved in this test (2.2×10^{-4} mbar) is sufficient for use in the cyclotron, where a more powerful vacuum pump is present.

4. First beam tests

4.1. Experimental Setup

After the successful preliminary and vacuum tests, the π^3 monitor was tested with the Bern medical cyclotron. For these measurements, the paper screen of the preliminary tests was replaced with a scintillating foil. Because of its thinness and coating, the foil is very fragile and special care needs to be used in the assembly. The beamline configuration used in all of the cyclotron tests is shown in Fig. 20.

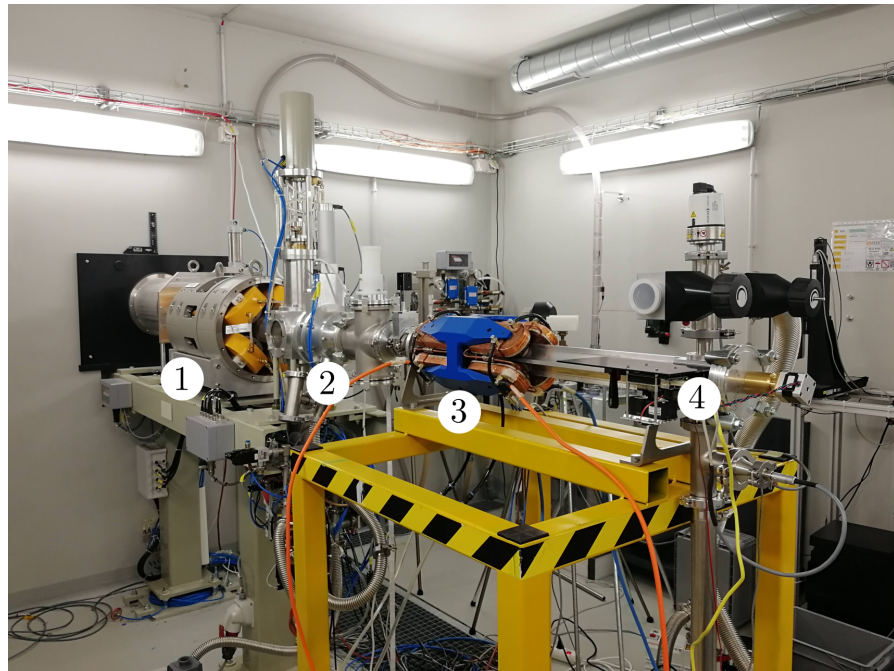


Figure 20: The setup for measurements with the Bern medical cyclotron.

Visible in the image is one of the BTL quadrupole doublets (1), the π^2 detector (2), the integrated magnets of the MBL (3) and the controller and motor of the π^3 monitor (4). Beam steering and focusing is possible using either the BTL magnets or the integrated magnets of the MBL. The magnets of the MBL can be moved for 350 mm along the MBL axis, depending on the requirements. The π^2 monitor was mounted ahead of the π^3 and used as a means to optimize the beam regarding focusing and positioning. For the measurements with the π^3 , small beam currents between 20 nA and 60 nA were used. In order to achieve this small beam current, the main coil current of the cyclotron was moved away from the resonance plateau.

4.2. Preliminary cyclotron testing

In June 2019, first measurements were carried out with the π^3 monitor. Because of a malfunction in the gravity puller system, only the first half of the MBL (in the direction of the beam) was able to be traversed. By moving the magnets of the MBL to the front, the visible effect of the MBL magnets was attempted to be maximized. Also, the scintillating foil was partially detached by the airflow when the system was pumped, as can be seen in Fig. 21b. Regardless, it was decided

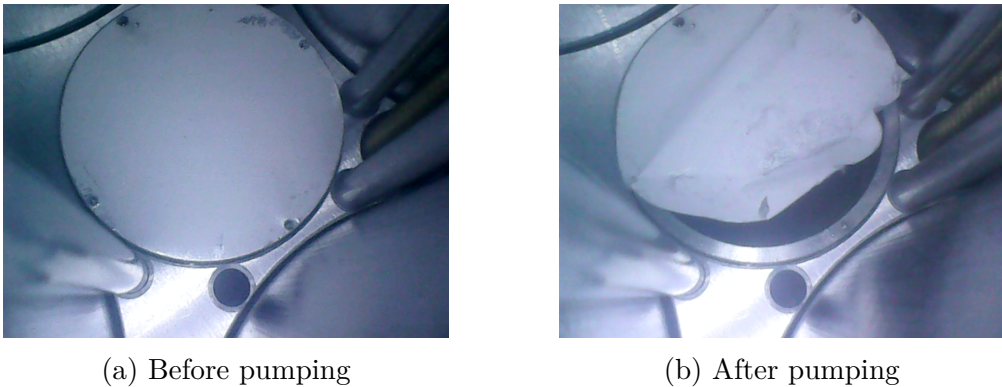


Figure 21: The scintillating screen inside the beamline before and after vacuum pumping.

to perform a test with this broken foil instead of reassembling the system with a new foil, because the measurement software and the effect of the proton beam on the electronics could still be evaluated. Also, the complete dis- and reassembly process is a very time consuming process of at least a half day. Fig. 22 shows the first picture taken by the π^3 monitor, which is overexposed. By reducing the beam current to 60 nA and using the BTL magnets in combination with the π^2 monitor to focus the beam, an adequate image usable for measurements could be obtained, as seen in Fig. 23.

Several different types of tests were conducted in the first measurement campaign. First, the beam was focused as well as possible, and beam profiles were obtained for the first half of the MBL. This first setup was equivalent to having a proton beam in drift space, as none of the MBL magnets were switched on. Next, the current of the steering magnets of the BTL was changed during the measurement in multiple steps while the monitor was moving to be able to measure the change of the beam center position. As a last test, the quadrupole magnets of the MBL were enabled and driven with a high current of 70 A to measure a non linear beam profile inside the MBL magnets.

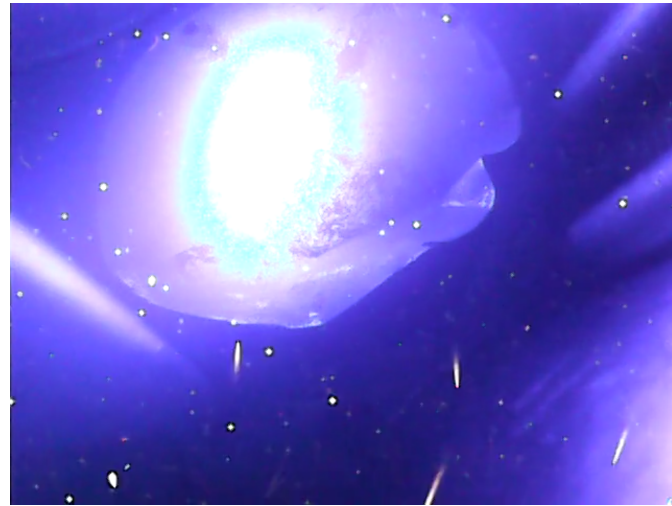


Figure 22: Image from the first measurements performed by the π^3 . Note the overexposure due to an excessive beam current of 360 nA and stray neutrons and protons appearing as white streaks in the image.



Figure 23: Still frame of the monitor after adjusting the beam current to 60 nA and focusing. The wrinkles and inhomogeneities in the coating of the foil can clearly be seen. Also, by the decreasing the beam current, the noise from stray neutrons and protons is reduced.

4.3. Results of the first measurement campaign

4.3.1. Beam in drift space

In a drift space, since there are no external forces acting on the beam, the beam trajectory of a particle in the beam is simply defined by

$$\Delta x, \Delta y = L \tan(\theta_{x,y}), \quad (4.3.1)$$

where $\Delta x, \Delta y$ is the change of the particle position in x and y , L is the length traveled inside the drift space and $\theta_{x,y}$ is the angle between the beamline axis and the beam trajectory in x and y . Therefore, it is expected that the standard deviation, which describes the beam width, is growing linearly with the distance inside of the drift space. Also, the beta function defined by $\beta = \sigma^2/\epsilon$, where σ is the standard deviation and ϵ is the beam emittance which stays constant, will increase quadratically inside the drift space.

For the first measurement, the beam was focused using the BTL magnets and the π^2 monitor to fit on the intact part of the scintillating screen at the top left. The currents used for the BTL magnets are given in table 1. The scintillating foil of the π^3 was then moved multiple times through the first half of the MBL between the 0 and 330 mm positions while video was recorded for every pass. Between the measurements, the beam was blocked by a shutter in order to minimize the exposure of the electronics to the beam and avoid unnecessary activation of the system components. This was also performed for the other measurements.

	1st. quadrupole doublet	2nd. quadrupole doublet	Steering magnets
Horizontal:	44.9 A	39.55 A	-0.47 A
Vertical:	47.3 A	25.5 A	0.2 A

Table 1: Settings of the BTL magnets used in this measurement.

Fig. 24 shows the position of the beam center throughout the first half of the MBL. The beam center moves linearly in the distance along the MBL axis and travels a total distance of 2.6 ± 0.3 mm in the horizontal direction, and a distance of 0.5 ± 0.3 mm in the vertical direction on the target screen. This distance traveled is measured after removing outliers with a moving average, which are caused by stray neutrons and protons appearing as white dots and streaks in the images. This means that the beam entered the drift space with an angle of $0.22 \pm 0.03^\circ$ with respect to the beamline axis. It is also possible that the MBL is slightly misaligned with respect to the beam axis, even though laser alignment was used.

Fig. 25 shows the standard deviation of the beam squared (σ^2) in both the vertical and horizontal plane. This squared standard deviation is directly proportional to the β -function, which describes the beam envelope by the transverse beam size evolution along the beamline axis. After removing outliers, the standard deviation varies by 2.8 ± 0.3 mm in the horizontal direction and by 1.0 ± 0.3 mm in the vertical direction.

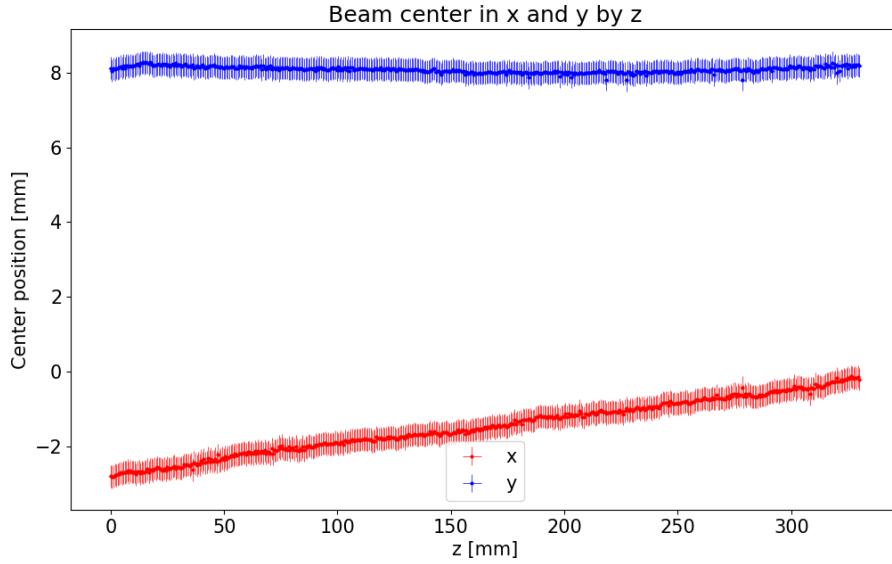


Figure 24: Position of the beam center in the horizontal (x) and vertical (y) plane along the distance inside the MBL (z) for a beam focused with the BTL magnets.

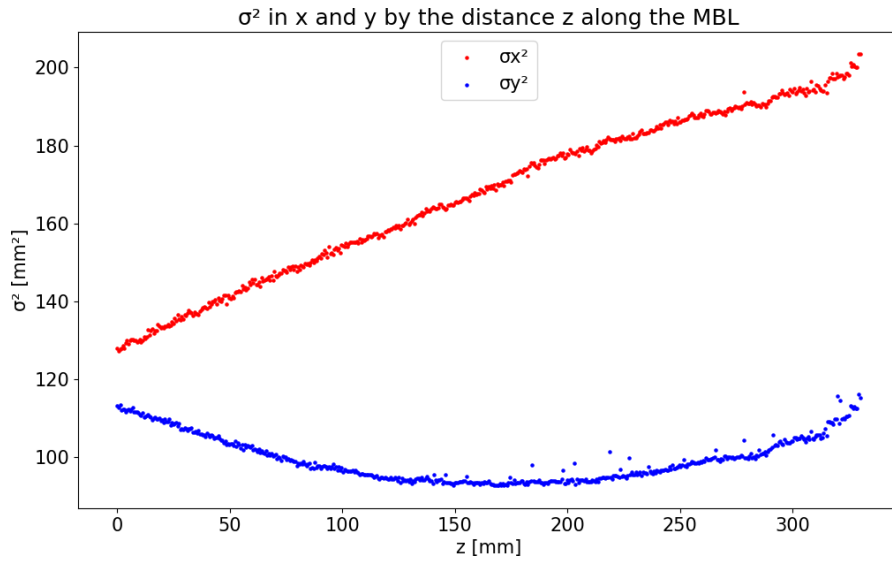


Figure 25: σ^2 , which is directly proportional to the β -function, in the horizontal and vertical plane for a beam focused with the BTL magnets.

4.3.2. Changing the current on the BTL steering magnet

For this measurement, the current of the horizontal steering dipole magnet of the BTL was changed manually during movement of the monitor in 7 steps, from a current of -2.27 A to -1.07 A . The effect of the steering magnet can clearly be seen in the horizontal position of the beam center, Fig. 26. When the steering current is not changed, the beam center moves with the same slope seen in the previous measurement (Fig. 24), caused by the misalignment of the beam to the beamline axis. The position in the vertical direction stays unchanged inside of the error bar and is not affected by the horizontal steering magnet.

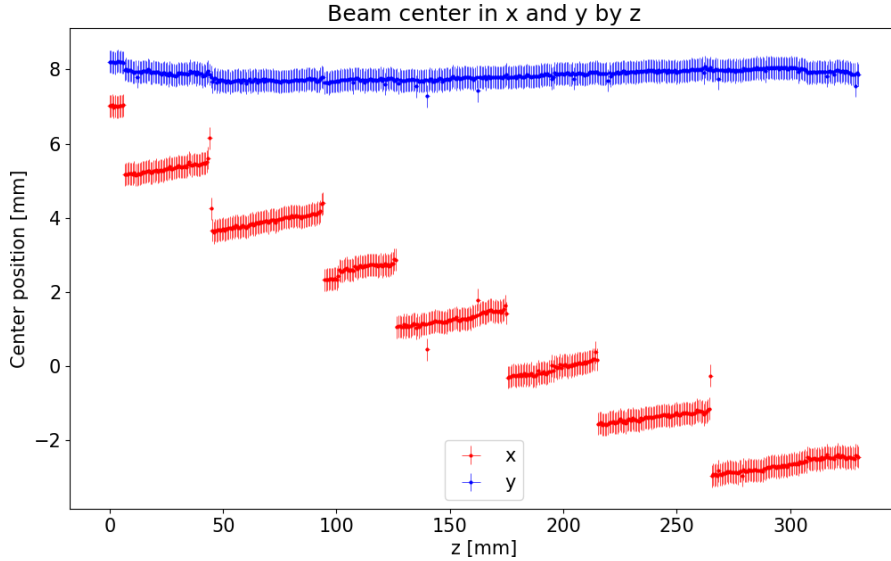


Figure 26: Position of the beam center in the first half of the MBL when changing the current of the horizontal steering magnet of the BTL.

In Fig. 27 the σ^2 is depicted, which is not exactly identical with the previous measurement at the beginning of the MBL because the center position and shape of the provided beam changes with time as the cyclotron warms up. The effect of the steering magnet can be seen in the σ^2 as small discontinuities when the steering current is changed. By moving the beam away from the center of the focusing quadrupoles, the steering dipole can have an effect on the beam shape. The standard deviation is more sensitive to stray protons and neutrons in the image than the analysis of the beam center position, which is why the noise is more intense in data of the σ^2 .

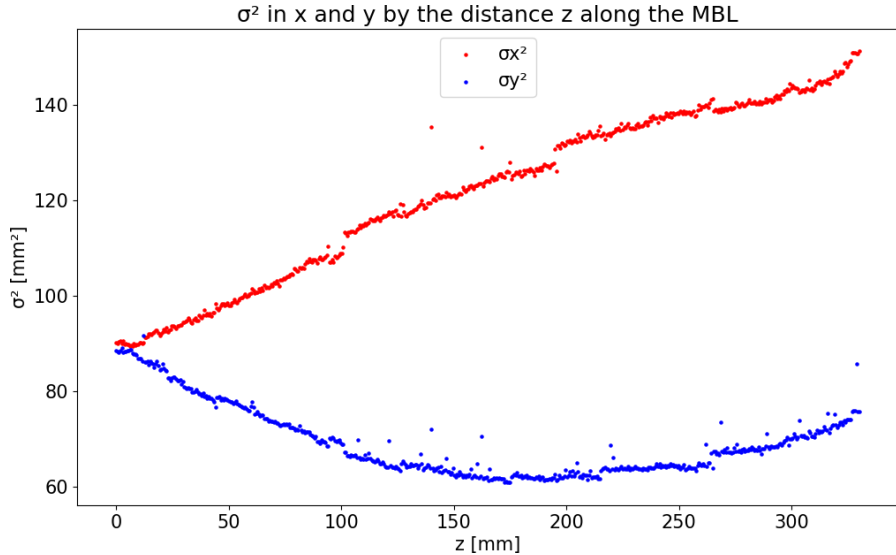


Figure 27: σ^2 in x and y while the steering current of the BTL magnets is changed.

4.3.3. Enabling the MBL focusing quadrupole

In the last measurement conducted, the magnets of the MBL were connected to the power supply and one of the focusing quadrupoles was driven with a current of 70 A to achieve focusing in the horizontal plane. The focusing and steering of the BTL magnet was changed for this measurement in order to keep the beam on the screen by compensating the effect of the MBL magnet, with the currents given in table 2. The movement of the beam center position (Fig. 28) is once again linear, but a discontinuity is clearly visible at around 80 mm. Since this discontinuity appears in both planes at the same time, it is because of the camera missing to record some frames, which can happen occasionally after extensive usage. Because the motor provides no feedback about the position but moves at a constant speed, the timestamp in the video is assumed to be directly correlated to the position and if the camera misses to record frames for a second, discontinuities can appear in the data.

	1st. quadrupole doublet	2nd. quadrupole doublet	Steering magnets
Horizontal:	50.4 A	38.6 A	-1.07 A
Vertical:	46.1 A	43.00 A	0.1 A

Table 2: Settings of the BTL magnets used in conjunction with the MBL magnets.

The standard deviation (i.e. the beam shape) now behaves differently from drift space, as expected. As seen in Fig. 29, the standard deviation in x decreases with focusing, while it increases slightly in the y axis. After removing the outliers, the standard deviation is decreased by 2.0 ± 0.3 mm in the horizontal direction and increased by 0.7 ± 0.3 mm in the vertical direction. Because the beam does not fit entirely on the intact part of the screen at the end of the distance moved, the noise in the standard deviation is increased.

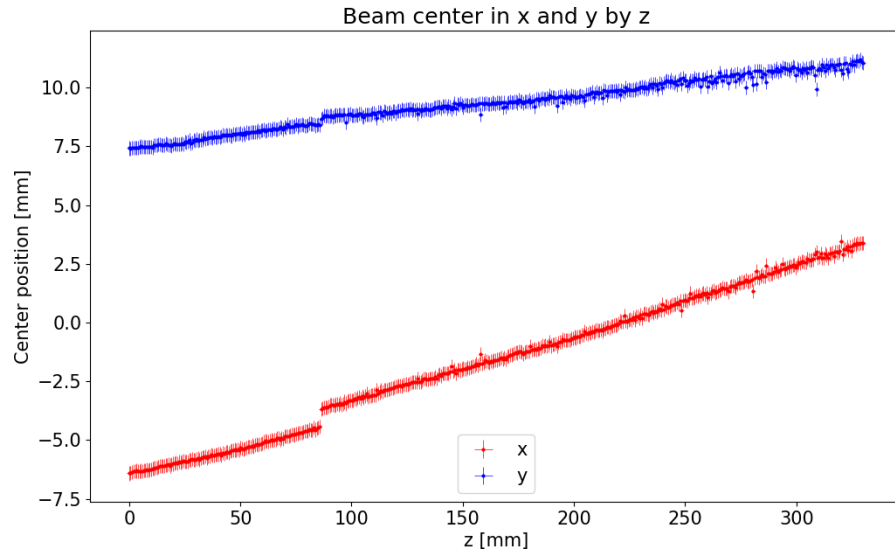


Figure 28: Position of the beam center with a MBL quadropole activated.

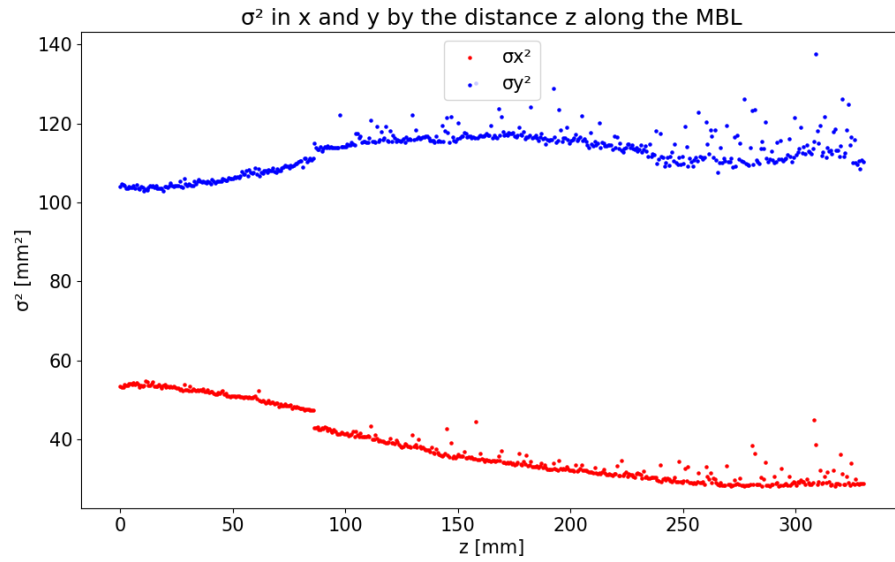


Figure 29: σ^2 inside the magnetic field of the MBL quadrupole magnet.

4.3.4. Discussion of the first measurement campaign

With the preliminary tests, first results and experience in using the π^3 monitor with a proton beam could be successfully obtained, which aided in optimizing the experimental parameters for future measurements. Three main issues were noticed during the analysis of these preliminary measurements, which are the following:

1. Avoid overexposure of the camera. If the camera pixels are saturated, the intensity profile of the beam will be cut off at the top, which can effect the accuracy with which the analysis software can fit a Gaussian to the profile. Also, in image preprocessing, the effect of the streaks of stray protons and neutrons is attempted to be minimized by utilizing a maximum threshold. If parts of the beam are at maximum pixel intensity, the stray proton and neutron streaks can not be removed without also removing part of the beam with this method.
2. Ensure that the beam is always fully contained on the target screen. Due to the limited intact area of the scintillating foil in the preliminary tests the beam could not be centered and parts of it could move off the screen. Also, the beam spot can only be focused down to a minimal size which can be large if far away from the focusing magnets. Therefore, it is advised to keep the beam spot as small and as centered as possible.
3. Ensure that the corner points of the scintillating screen are aligned exactly to the beam axis and that the screen itself and its coating are as intact as possible. Because of the inaccuracies of manual mounting, a small error in the rotational angle of the scintillating screen can be present, which can impact analysis by leading to incorrect perspective correction.

4.4. Results of the second measurement campaign

In August 2019, the π^3 prototype was able to be tested in a fully functional condition during the second measurement campaign. In order to avoid the damage of the foil during pumping, more venting holes were drilled into the support mount of the scintillating foil to facilitate air movement. Also, the vacuum pumping and venting process was modified. Previously, the vacuum inside the MBL was handled by the BTL vacuum system, which uses a butterfly valve to try and slow the airflow during the first parts of the pumping process.

In the new setup, depicted in Fig. 30, a manual gate valve (1) was installed between the π^2 exit and the MBL entrance, allowing to pump the BTL vacuum and the MBL vacuum system in two different steps with different speeds. To pump the MBL system, a separate roughing pump and turbo pump (2) were used in combination with a valve (3) which heavily restricts the airflow during the initial pumping.

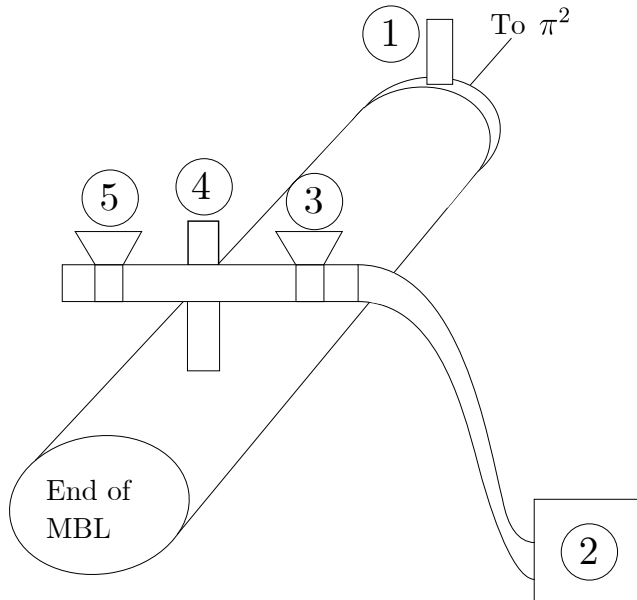


Figure 30: Sketch of the MBL with the improved vacuum system attached.

This valve is opened slowly at first, until a vacuum of 10^{-3} mbar is reached using the roughing pump. The pressure inside the MBL can be measured by a vacuum gauge (4) attached to the MBL. As soon as this low vacuum is reached, the valve is opened fully and the turbo pump is started. After a high vacuum of around 10^{-5} mbar is reached, the BTL side is also pumped to high vacuum and the gate valve in between is opened to connect both vacuum systems and allow passage of the beam. For venting, the gate valve is closed again and the MBL venting valve (5) can be used to increase the pressure inside the MBL. With this new system in place, damage to the foil could be successfully avoided.

Also, the previous issue with the gravity puller system was able to be resolved, and the total length of the MBL was able to be used in these measurements. By using a low beam current of 20 nA, overexposure of the foil could be avoided and less stray protons and neutrons hit the camera, reducing the image noise.

4.4.1. Beam focused by the BTL in drift space

In the first measurement, the BTL magnets were used to focus the beam at the entrance to the MBL, while the MBL magnets remained inactive. The currents used for the magnets of the BTL are given in table 3. In this drift space, the monitor was moved from 0 mm to 660 mm multiple times, and the measurement with the least amount of dropped frames was chosen.

	1st. quadrupole doublet	2nd. quadrupole doublet	Steering magnets
Horizontal:	50.4 A	38.6 A	-2.27 A
Vertical:	46.1 A	43 A	0.80 A

Table 3: Settings of the BTL magnets used to focus the beam before drift space.

The position of the beam center Fig. 31 behaves linearly inside the error bar and moves 3.7 ± 0.3 mm in the horizontal and 2.0 ± 0.3 mm in the vertical plane. This means that the beam entered the MBL with a small angle of $0.36 \pm 0.03^\circ$ relative to the beamline axis. Fig. 32 shows the σ^2 inside the MBL. The σ^2 slowly increases quadratically, but is damped towards the end of the MBL, when the beam size approaches the size of the scintillating foil and is cut off.

With the measured beam shape and beam center position, a 3D representation of the beam envelope along the MBL can be created by plotting 1- σ ellipses at every measured position along the MBL, as explained in chapter 2.2.3. This 3D representation is shown in Fig. 33 and from another perspective in Fig. 34. Both of these 3D beam envelopes show the cone-like behavior of the beam inside drift space.

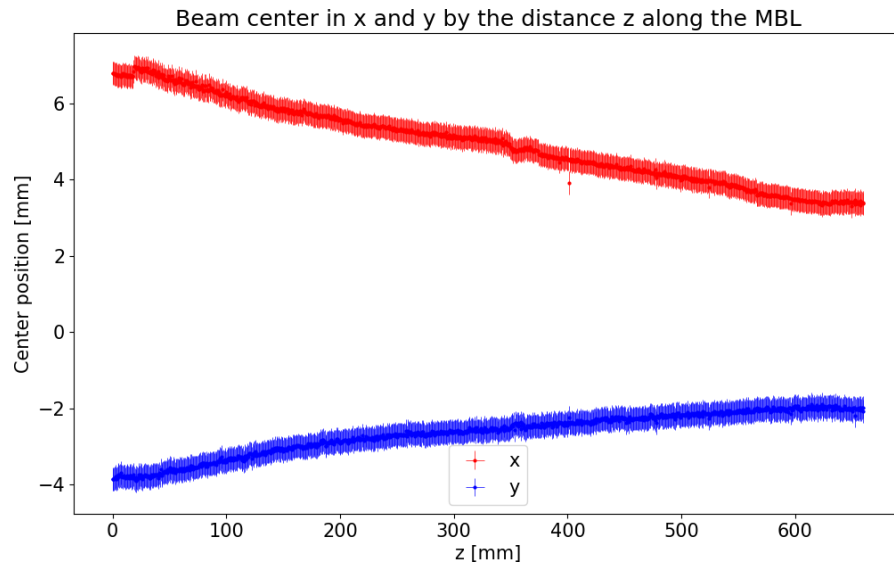


Figure 31: Position of the beam center in the horizontal (x) and vertical (y) axis along the MBL.

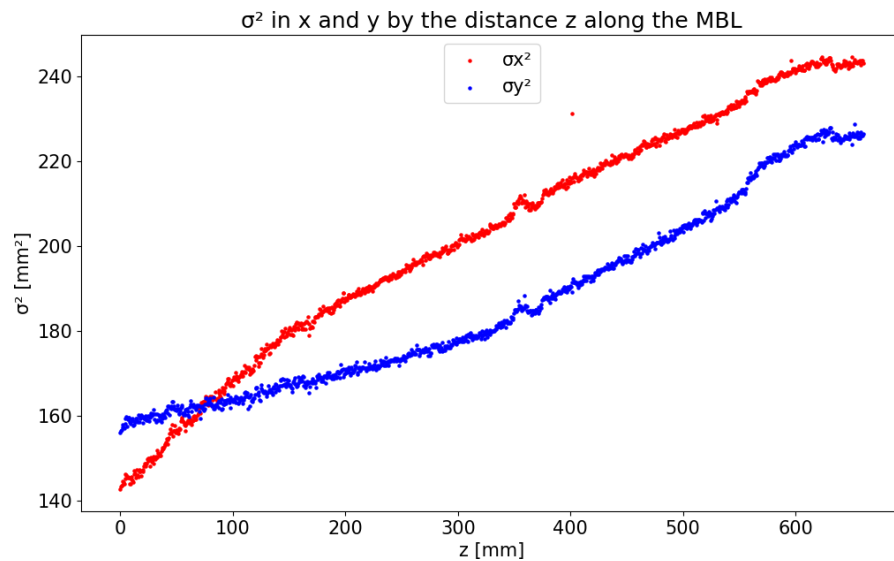


Figure 32: σ^2 of the beam in both axis along the MBL.

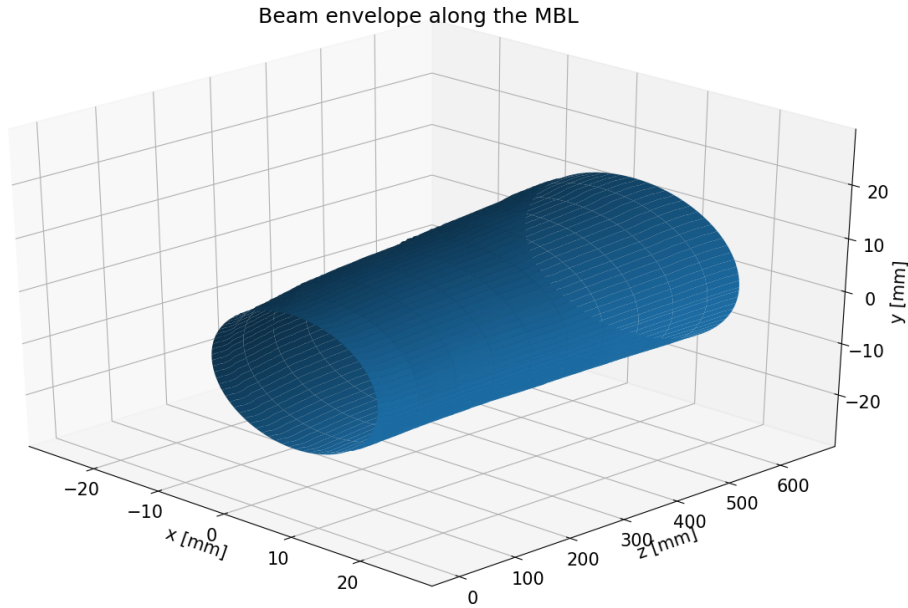


Figure 33: 3D representation of the beam envelope along the MBL. The horizontal (x) and vertical (y) axis are not the same scale as the axis z along the MBL.

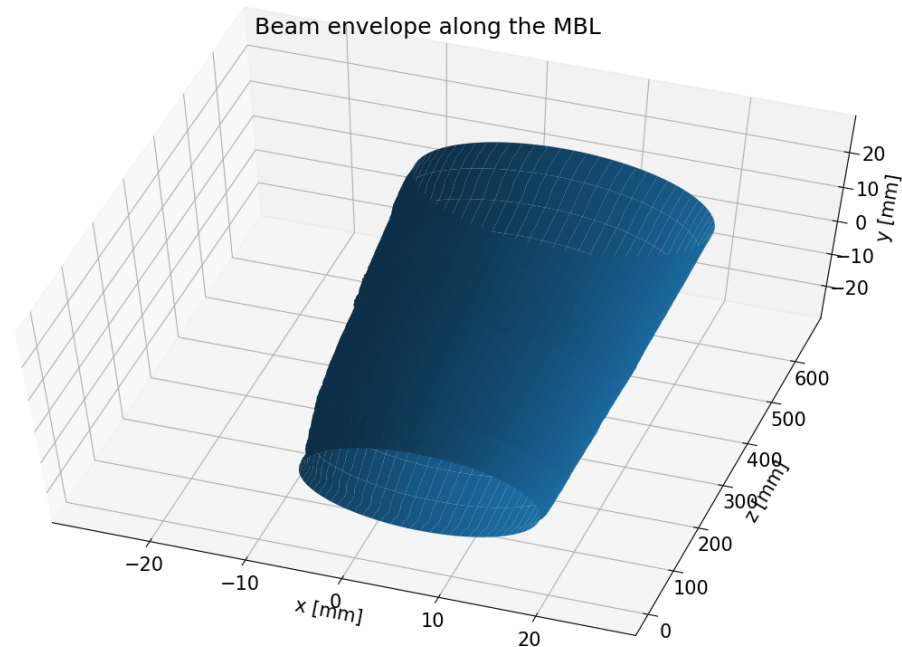


Figure 34: 3D representation of the beam envelope from another perspective.

4.4.2. Focused beam being refocused by the MBL magnets

The beam was then focused at the MBL entrance and refocused by the MBL magnets, which were driven with a current of 40 A on both quadrupoles. To focus the beam at the entrance of the MBL, the currents in table 4 were used for the BTL magnets.

	1st. quadrupole doublet	2nd. quadrupole doublet	Steering magnets
Horizontal:	49.6 A	35.9 A	-1.47 A
Vertical:	47.1 A	33.8 A	0.50 A

Table 4: Settings of the BTL magnets used to focus at the MBL entrance.

Because the beam was not perfectly centered inside the MBL quadrupoles, a steering effect is observed as a movement of the beam center position (Fig. 35). Nevertheless, the center position moves only 0.6 ± 0.3 mm in the horizontal and 1.3 ± 0.3 mm in the vertical axis, which means that the beam was aligned quite precisely to the MBL axis.

The σ^2 inside the MBL clearly shows the effect of the MBL quadrupoles. First, the beam is focused in the horizontal plane and gets defocused in the vertical plane. Because the beam size is already very small as it enters the MBL, the MBL magnets can not focus the beam in the horizontal plane much further. After the beam has passed the first quadrupole, it gets focused in the vertical plane and defocused in the horizontal. With the beam being defocused in one plane as it is focused in another, the effect of Louisville's theorem [11] is distinctively visible. The beam waist of the horizontally focusing quadrupole is visible at around 200 mm, but for the vertically focusing quadrupole, no single beam waist can be identified in the data.

In Fig. 37 and Fig. 38 the 3D representation of the beam envelope is reported, which distinctively shows the horizontal focusing and vertical defocusing in the first half of the MBL. After the horizontal focusing, the vertically focusing quadrupole circularizes the beam. In total, the beam size was increased instead of decreased by the MBL magnets.

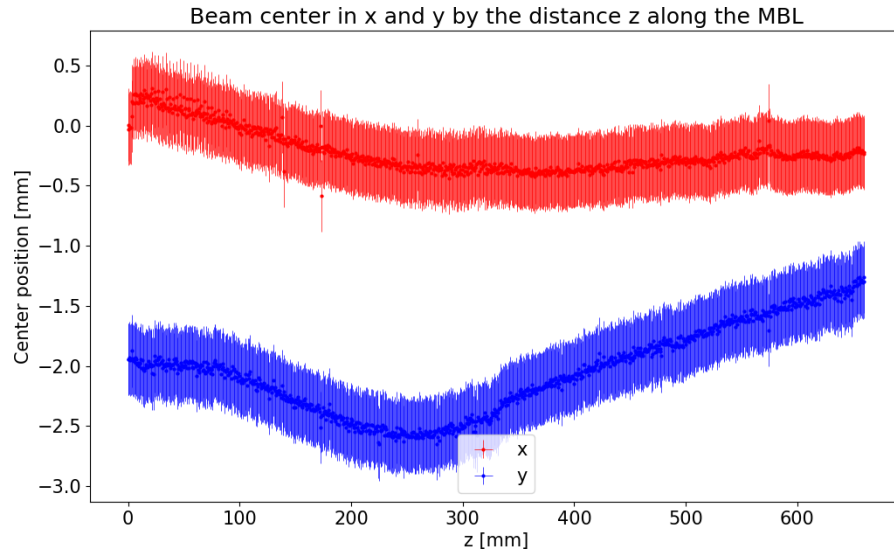
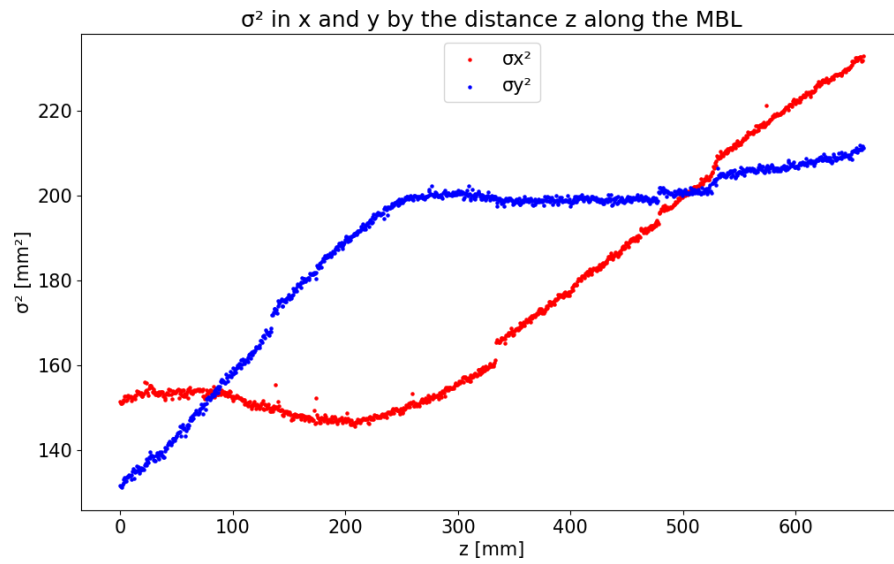


Figure 35: Position of the beam center along the MBL.

Figure 36: σ^2 of the beam in both axis along the MBL.

Beam envelope along the MBL

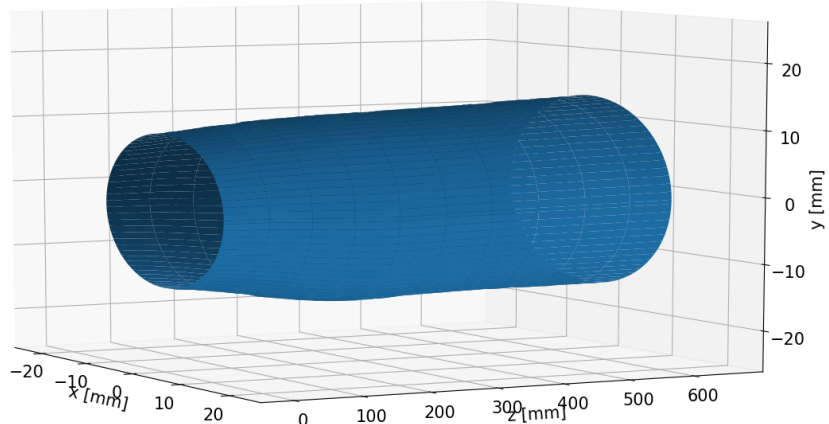


Figure 37: 3D representation of the beam envelope along the MBL.

Beam envelope along the MBL

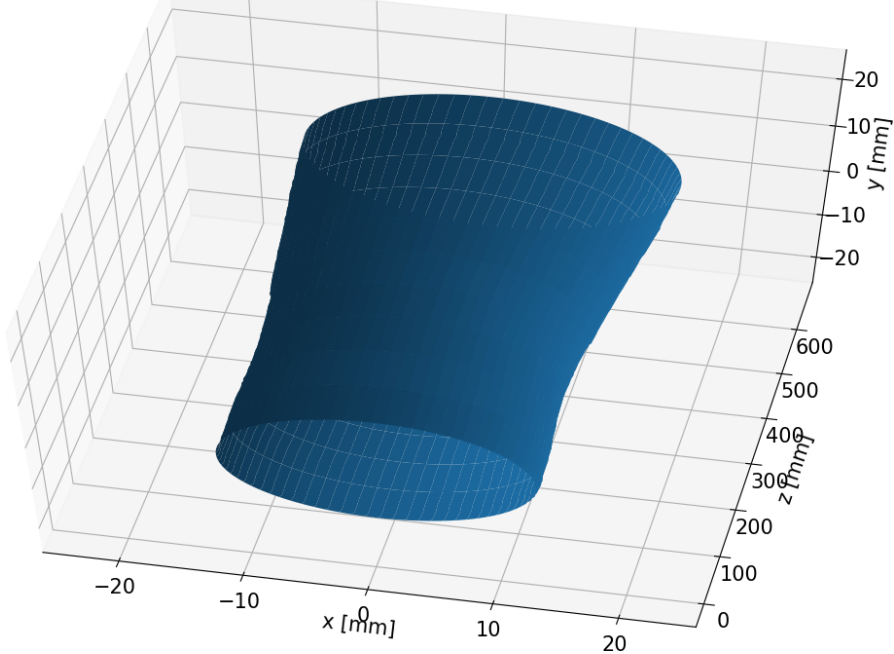


Figure 38: 3D representation of the beam envelope from another perspective.

4.4.3. Flat beam being focused by the MBL magnets

In this measurement, the focusing magnets of the BTL, which were in use for all previous measurements, were set to only very small currents given in table 5. With these small currents, the BTL magnets have no significant focusing or defocusing effect, resulting in an uniformly spread beam, covering the entire scintillating foil and its surroundings. This "flat" beam was then attempted to be focused using the MBL magnets, using a current of 75 A. Fig. 39 shows the movement of the beam

	1st. quadrupole doublet	2nd. quadrupole doublet	Steering magnets
Horizontal:	33 A	0.5 A	-1.47 A
Vertical:	33 A	0.5 A	0.50 A

Table 5: Settings of the BTL magnets used to focus at the MBL entrance.

center inside the MBL, which is not linear, as the quadrupoles of the MBL have a steering effect on the beam because the beam was not exactly centered inside the quadrupole. Also, there are discontinuities visible, which are caused by the camera missing frames.

Fig. 40 shows the σ^2 in both planes and Fig. 41 and Fig. 42 show the 3D beam envelope inside the MBL. The beam is immediately focused in the horizontal axis, down to a very narrow standard deviation of 11.5 ± 0.3 mm at a distance of 330 mm, which can be distinctively seen in the 3D beam envelope. Because the beam does not fit on the screen anymore and is cut off vertically during the horizontal focusing, the effect of the vertical focusing can not be seen in its entirety. With the MBL magnets, a flat beam covering the entire image was able to be focused to fit on the target screen.

These results show that the π^3 monitor can successfully be used to measure the beam envelope of a proton beam with a high spatial resolution of 0.03 mm in the horizontal and vertical plane and a resolution of 1 mm along the beamline axis. With this monitor, the effects of different magnets on a proton beam can be studied and understood.

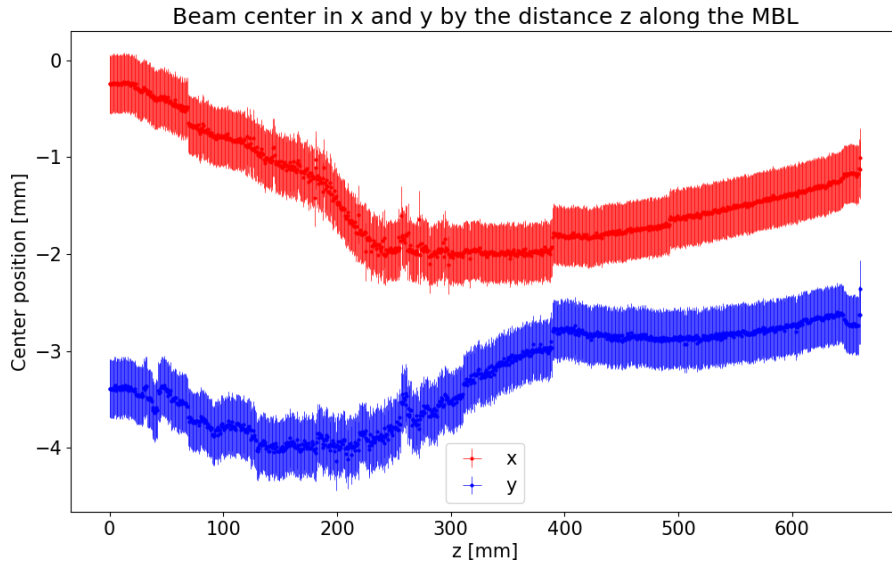


Figure 39: Position of the beam center along the MBL. A discontinuity can be seen at around 380 mm, caused by the camera missing frames.

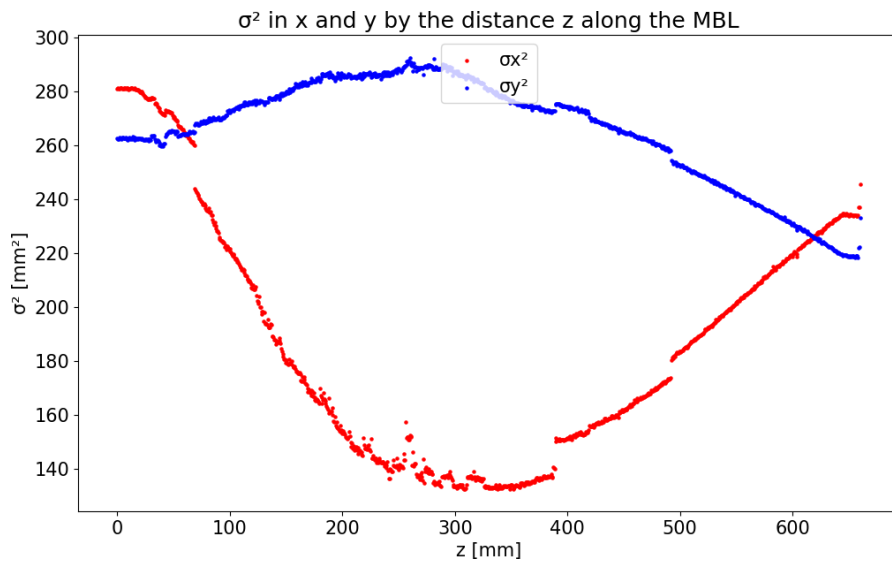


Figure 40: σ^2 in the horizontal and vertical plane for a flat beam being focused by the MBL magnets. The same discontinuity as in the beam center position can also be seen in this data.

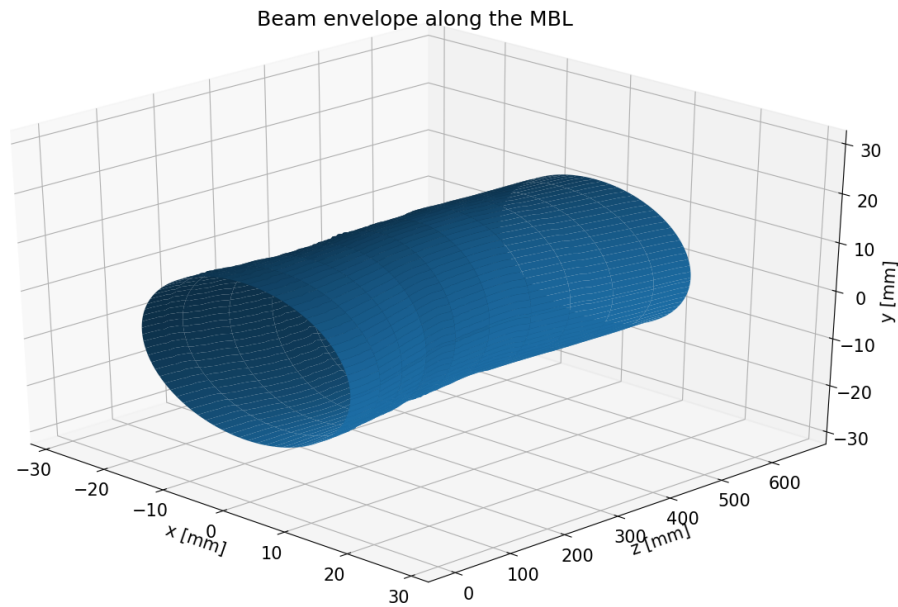


Figure 41: 3D representation of the beam envelope along the MBL.

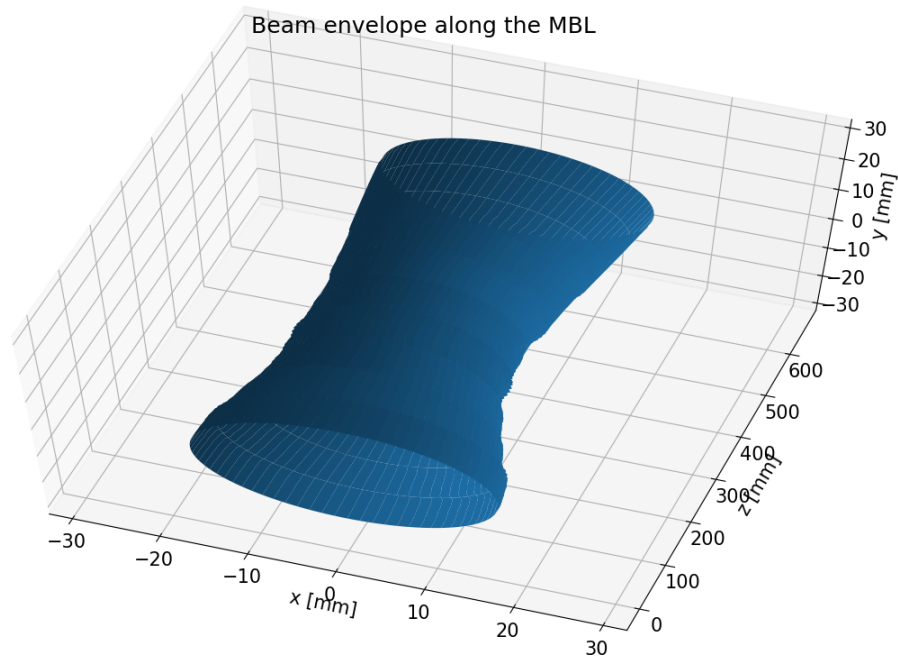


Figure 42: 3D representation of the beam envelope from another perspective.

4.5. Possible improvements to the π^3 detector

The measurements at the Bern medical cyclotron, suggested possible improvements to the system. First, the quality of the scintillating foils should be improved to increase their stability during vacuum pumping and to provide a more uniform coating. By using a support mount with a bigger surface to glue to the scintillating foils, the quality of the bond and therefore the foil's stability can be improved and the π^3 monitor could possibly be used without requiring a separate vacuum solution.

Furthermore, by using scintillating foils of different conversion efficiencies, beams with a higher currents could possibly be measured. But with higher currents, the radiation hardness and thermal properties of the camera have to be further investigated. The corner points necessary for image preprocessing can be marked permanently on the support mount itself instead of the scintillating foils, which removes the need to repeatedly create these points for every new foil. Also, by leaving the foil intact in its entirety, more of it can be used to detect the beam.

Another area where large improvements are possible is in the camera used to view the beam. Increasing the camera resolution can provide immense improvements to the detector resolution. For example, by using a camera able to record in 4K ($3840 \text{ px} \times 2160 \text{ px}$), the detector resolution increases more than fourfold. Also, if a camera with manual ISO and exposure time control were to be used, then also the linearity of the monitor in relation to the beam current could be established, as has been done with the π^2 monitor [7].

Using a camera which can record more frames per second increases the resolution along the MBL axis or enables a faster motor to be used while keeping the same resolution and decreasing the time needed to perform a measurement. Currently, space restrictions are the most important criteria for the camera choice and more performant (while still being inexpensive enough to be considered expendable) camera models have to be found.

The hardware components of the π^3 responsible for moving the scintillating foil can be improved to reduce vibrations and to simplify the mounting process.

In general, the π^3 monitor could be adapted also to other types of beamlines than the Mini PET-beamline, for example to the KF-40 format, as long as the mechanical components of the π^3 can be constructed in appropriate dimensions. By adapting to different types of beamlines, the π^3 can be used to study many different already existing beamlines and magnets.

On the software side, there is still work left to provide an easy to use and reliable control software. By implementing a GUI (graphical user interface) the required knowledge to operate the π^3 can be reduced. Also an unified solution combining all parts of controlling the π^3 (video capture and moving the monitor) could be constructed. With an unified software solution, the position of the scintillating foil in the MBL can be kept track of automatically and invalid user inputs, beyond the limits the foil can move without damage, can be avoided.

At the moment, the preprocessing still requires manual tweaking and finding optimal parameters to analyze a measurement, but an unified software would be able to automatically save or calculate at least some of the parameters, for example

the distance the monitor moved or cut the video of the measurement to the timestamp the motor starts moving. Also, a live view and analysis of the beam during measurement can be helpful in controlling the π^3 monitor during a measurement, but the performance of the Raspberry Pi used to control the π^3 monitor might be insufficient for this. Further image preprocessing techniques such as object removal could be employed in the image preprocessing to remove stray protons and neutrons in the images.

One of the main drawbacks of the π^3 prototype is the long measurement time of up to 3 min, which is caused by the limited speed of the motor. During the measurement time, the provided beam of the cyclotron can change and disturb the measurement. With a faster motor and a camera with a higher frame rate, the measurement time could be decreased while still retaining the same resolution, but the vibrations during movement will also increase with increased movement speed. Different mechanical solutions to enable faster movement without excessive vibrations could be investigated.

5. Conclusions and outlook

The first π^3 detector prototype was built and successfully tested. Preliminary testing showed that the π^3 features a spatial resolution of 0.3 mm in the horizontal and vertical axis and a resolution of 1 mm along the beamline axis. Beam tests at the Bern medical cyclotron showed that the system was successfully able to measure the beam center position and beam shape throughout the length of the Mini-PET beamline (MBL). The effect of the beam transfer line and the MBL magnets were studied and 3D representations of the beam envelope inside of the MBL were obtained for different settings of the magnets.

All electronic components of the detector exposed to radiation are low cost (< 100\$) and consumer-grade, but radiation hardness did not prove to be a problem in the measurements. The only expensive part of the detector, the scintillating foil, can be used for multiple measurements and does not suffer any damage from vacuum pumping with the modified setup.

Points to improve still exist for the π^3 monitor. The complete mounting process of the monitor to the MBL is a time consuming process, requiring at least half a day. The camera used for this prototype is not reliable enough and can miss frames during a measurement, leading to missing data. Also, no manual ISO and exposure time control is available, so the linearity of the monitor in relation to the beam current was not able to be evaluated. Because of the long time needed to perform a measurement (3 min), the beam provided by the cyclotron might change during the measurement.

Beam parameters measured by the π^3 could be used to verify the accuracy of beam transport simulations. With one measurement of the π^3 being composed of around 1000 individual beam cross sections, much more data points are available than in measurements using multiple traditional beam monitors.

Another direct application of the π^3 exists in the production of radioisotopes at the Bern medical cyclotron. Currently, to irradiate targets inside the solid target station (STS), the directly outputted beam of the cyclotron is used without any focusing. These targets have a size of about 6 mm, but the beam provided by the cyclotron has a size of 12 mm to 20 mm, meaning that only a small part of the beam hits the target and most of it is being wasted. Plans exist to optimize this process by using the MBL to focus the beam, as it is the only available option fitting the space requirements inside the cyclotron bunker. In order to optimize and understand the effect of the MBL magnets on the beam in this situation, the π^3 detector is a highly valuable tool, providing direct feedback of the beam shape and position throughout the MBL. Also, the data provided by the π^3 can be used to verify and enhance beam transport simulations in this application.

Altogether, the first prototype of the π^3 monitor shows very promising results, with the measurements providing an accurate and unique view of the beam not possible before and the results obtained in the framework of this thesis will serve as the basis for further development of this innovative instrument.

Acknowledgments

First, I would like to thank my supervisor Prof. Dr. Saverio Braccini for his helpful tips and guidance. Also, i would like to thank him for making this thesis possible by coming up with the idea for the π^3 together with Dr. Tommaso Carzaniga.

Next, I would like to thank Dr. Carolina Belver for the immense help and valuable feedback in all parts of the thesis, from developing the detector software, to helping conduct the experiments to writing the thesis.

Thanks to the team of the LHEP workshop, the π^3 monitor was able to be built. In particular, I would like to thank Pascal Lutz from the LHEP workshop for his tireless help building and explaining the mechanical and electrical components of the π^3 monitor and for his valuable help in the experiments conducted.

Finally, I would like to thank Phillip Häffner for aiding in the measurements at the Bern medical cyclotron.

References

- [1] M.K. Craddock. “Eighty years of cyclotrons”. In: *Proceedings of CYCLOTRONS 2010* (Lanzhou, China). 2010. URL: <http://web.archive.org/web/20190822085622/https://accelconf.web.cern.ch/accelconf/Cyclotrons2010/papers/mom1cio02.pdf>.
- [2] Ernest O Lawrence. “Method and apparatus for the accelerations of ions”. US patent 1948384A. Feb. 1932.
- [3] Saverio Braccini. “Particle Accelerators and Detectors for medical Diagnostics and Therapy”. Habilitation Thesis. University of Bern, Apr. 2013.
- [4] *Mini-PET beamline*. D-Pace Inc., 2019. URL: <http://web.archive.org/web/20190822085929/https://www.d-pace.com/?e=51>.
- [5] R. Dölling. “BEAM DIAGNOSTICS FOR CYCLOTRONS”. In: *Proceedings of CYCLOTRONS 2010* (Lanzhou, China). 2010. URL: <http://web.archive.org/web/20190830145723/https://accelconf.web.cern.ch/AccelConf/Cyclotrons2010/papers/wem2cio04.pdf>.
- [6] M. Auger et al. “A detector based on silica fibers for ion beam monitoring in a wide current range”. In: *Journal of Instrumentation* 11.03 (Mar. 2016), P03027–P03027. DOI: [10.1088/1748-0221/11/03/p03027](https://doi.org/10.1088/1748-0221/11/03/p03027).
- [7] Matthias Schmid. “Development and Optimization of a Two-Dimensional Beam Monitoring Detector at the Bern Medical Cyclotron Laboratory”. Bachelor’s Thesis. University of Bern, Feb. 2018.
- [8] Meinrad Schefer. “Study of a novel two dimensional online beam monitoring detector”. Bachelor’s Thesis. University of Bern, Jan. 2018.
- [9] *Phosphor Screens*. ProxiVision, Jan. 2016. URL: <http://web.archive.org/web/20190822090315/https://www.proxivision.de/product/scintillating-screens/>.
- [10] Jemellie Galang et al. *A Green Laser Pointer Hazard*. 2010. eprint: arXiv: 1008.1452.
- [11] B.J. Holzer. “Introduction to Transverse Beam Dynamics”. In: arXiv:1404.0923 (Apr. 2014), 27–45. 19 p. DOI: [10.5170/CERN-2013-007.27](https://doi.org/10.5170/CERN-2013-007.27).
- [12] *Proceedings of CYCLOTRONS 2010* (Lanzhou, China). Sept. 2010.

Appendices

A. Source code

The source code used to control the monitor and analyze the conducted measurements can be found in <https://github.com/prakhub/pi3> and is licensed under the MIT License.

B. Manual of the π^3 detector

B.1. Setup

First, setup a Raspberry Pi with the Raspbian operation system and make sure there is a way to connect to the Raspberry Pi. Connecting to the Raspberry Pi can be either done via command line using `ssh -X pi@ip-address` or graphically via VNC. The `-X` option allows for X passthrough, meaning that windows created by the Raspberry Pi can be displayed also get routed via `ssh` and displayed on the computer connecting to the Raspberry Pi. It is recommended to connect via command line which has lower latency. The Raspberry Pi needs a power source of 24 V with a current limit of at least 3 A, which is required for the motor. Clone or download the git directory (see chapter A) and make sure that `python3` is installed and used as default. Install the python packet manager `pip`¹⁰ and use it to install the software requirements of the π^3 software with `pip install -r requirements.txt`. The library `RPIO` might need to be installed manually from <https://github.com/metachris/RPIO>, using the v2 git branch. Also, `ffmpeg`¹¹ has to be installed in order to record and re-encode video with the Raspberry Pi.

After the software is setup, make sure that all components (USB camera, LED light and contact sensor) are properly connected and reachable by the Raspberry Pi.

B.2. Performing a measurement

All scripts used in the following can be found in repository of the source code (see appendix B) and the programs used to control the Raspberry Pi are found in `/bachelor-code/raspi`. A simple script to display a live view of the π^3 's camera can be run with the command `python3.5 simple_camera.py`. The camera light is controlled by the Raspberry Pi's PWM controller and can be enabled by executing `python3.5 -i led.py`. By modifying the duty cycle of the PWM object (`p.ChangeDutyCycle(newDutyCycle)`), the intensity of the light can be adjusted. With the light enabled and the screen being visible, a picture or a small video of the screen should be created, in order to find the corner points on the screen, later used in the analysis. Video can be recorded with the command

¹⁰<https://pip.pypa.io/en/stable/installing/>

¹¹<https://ffmpeg.org/>

`sudo ffmpeg -f v4l2 -framerate 8 -video_size 640x480 -input_format yuyv422 -i /dev/video0 -c copy filename.mkv` and stopped by pressing the key 'q', where `filename.mkv` is the path where the video is saved. This command records video in a raw format, because the Raspberry Pi is not powerful enough for simultaneous recording and video encoding, leading to missed frames. The raw file format can create very large file sizes of up to multiple GB and needs to be re-encoded and compressed with the command

```
sudo ffmpeg -i in.mkv -c:v libx264 -crf 27 -preset medium -pix_fmt yuv420p -y out.mkv,
```

where `in.mkv` is the path of the raw video, and `out.mkv` is the path to store the compressed video in. This reencoding can also be performed on another device where `ffmpeg` is installed. With a picture or video of the screen corner points saved, the LED lights can be turned off and a measurement can be performed.

Using `python camera.py` a simple live view of the camera can be obtained, which is useful for beam alignment. In combination with other beam monitors mounted ahead of the π^3 , the beam can be centered and focused until the desired beam is achieved. The π^3 can be moved inside the MBL using the command

```
sudo python old_motor.py -dirctrl=0 -pwmf=1 -pwmj=0 -sm=8 -dist=<mm> -step=<qty> 2>&1 >/dev/null.
```

The parameters for movement are: `dirctrl`, which specifies the direction the monitor moves in. A value of 0 moves the monitor to the motor at the end of the MBL, and a value of 1 moves the monitor into the direction of the cyclotron. The parameter `dist` controls the distance to move in mm and `step` controls in how many steps the movement will be completed. In almost all cases, `step` can be left as 1 to achieve a single, smooth movement throughout the desired distance. The other parameters relate to technical details of the PWM controller and don't need to be adjusted.

To perform a measurement, a video recording is started first and the command to move the monitor is sent afterwards. As soon as the movement is finished (command terminates), the recording can be stopped and saved. It is recommended to only open the beam shutter during measurements to minimize heating of the foil and radiation exposure. Also, the recordings of the measurements should be transferred to a local computer immediately after recording to avoid any data loss. An easy way to copy data over ssh is to use the secure copy protocol (`scp`). In order to avoid collision of the monitor with the ends of the MBL, special care has to be taken to note down the position of the monitor after every movement or to perform a homing operation if the position is not known.

Automatically keeping track of the position and stopping invalid user commands is a feature which is planned to be implemented in the future.

B.3. Preparing the analysis

In order to analyze a measurement correctly, it is important to adjust and modify the preprocessing parameters. All of the preprocessing parameters are stored in a file, called `metadata.txt` and are described in table 6. This file is read by the preprocessing script when executed and is to be placed in the same directory as

<code>self.points</code>	The pixel coordinates of the corner points on the screen
<code>self.distance</code>	The z-distance the monitor was moved
<code>self.color</code>	The color to extract during preprocessing (BGR indices)
<code>self.cutFrames</code>	Indices of the video frames to consider in analysis
<code>self.max_threshold</code>	Value of the maximum threshold
<code>self.min_threshold</code>	Value of the minimum threshold
<code>self.offset</code>	Image padding size in px
<code>self.radius</code>	Radius of the circular mask in px

Table 6: The parameters used in preprocessing.

the measured video file. A parameter which needs to be adjusted for every measurement is `self.cutFrames`, depending on how accurate the video capture can be synchronized with the movement of the screen. Also, `self.distance` needs to be specified for every measurement. The other parameters generally do not need to be changed during a measurement series, if the beam intensity stays constant and the screen is not disarranged by hand. A sample file containing the preprocessing parameters can be found in `bachelor-code/analysis/metadata.txt`.

B.4. Analyzing measurements

A sample script to analyze the measurements can be found in the file `main.py`, which includes the steps necessary to preprocess and analyze a measurement. Many premade plots for different parameters in different views exist in the `plots.py` module.